Multiparton scattering amplitudes with heavy quarks: calculational techniques and applications to diffractive processes

Ozeren, Kemal

Multiparton Scattering Amplitudes with Heavy Quarks: Calculational Techniques and Applications to Diffractive Processes

A thesis presented for the degree of

Doctor of Philosophy

by

Kemal Ozeren

Institute for Particle Physics Phenomenology

University of Durham

July 2008

Durham University

Abstract

In this thesis, we demonstrate the use of twistor inspired methods in the calculation of gauge theory amplitudes. First, we describe how MHV rules and the BCF recursion relations can be used in QED. Then we apply BCF recursion to the problem of amplitudes with massive fermions in QCD, using the process $gg \to bbg$ as an illustration.

Central exclusive production is a promising method of revealing new physics at the LHC. Observing Higgs production in this scheme will be hampered by dijet backgrounds. At leading order this background is strongly suppressed by a $J_z = 0$ selection rule. However, at higher orders there is no suppression and so it is important to calculate the contribution to the cross section of these terms. Among the necessary theoretical inputs to this calculation are the loop corrections to $gg \to bb$ and the amplitude describing the emission of an extra gluon in the final state, $gg \to bbg$. We provide analytic formulae for both these ingredients, keeping the full spin and colour information as is required.

Acknowledgements

I must first of all thank my supervisor James Stirling for his guidance and advice. I am also indebted to Nigel Glover, Adrian Signer and Valery Khoze for correcting my various misunderstandings and to the entire IPPP for providing such a great place to work and study.

I have been lucky to fall in with a good crowd: James, Martyn, John, Liz and Simon have been great housemates and made my four years in Durham happy and enjoyable. I also salute my office mates over the years - Gareth, Karina, Martyn, Ciaran and Stefan. A special mention goes to Emma for her love and support, and for putting up with me.

This thesis is dedicated to my parents, without whom it would not have been written. They taught me everything, and everything I achieve is thanks to them.

Declaration

I declare that no material presented in this thesis has previously been submitted for a degree at this or any other university.

The research described in this thesis has been carried out in collaboration with Prof W. James Stirling and has been published as follows:

- *MHV Techniques for QED Processes*,
  Kemal Ozeren and W. James Stirling
  JHEP **0511** (2005) 016 [arXiv:hep-th/0509063].

- *Scattering amplitudes with massive fermions using BCFW recursion*,
  Kemal Ozeren and W. James Stirling
  Eur. Phys. J. C **48** (2006) 159 [arXiv:hep-ph/0603071].

Contents

List of Figures

Chapter 1

Introduction

1.1 Basics of pQCD

Quantum Chromodynamics (QCD) is an $SU(N)$ gauge theory describing quarks and gluons with $N = 3$. It is part of the Standard Model of elementary particle physics. Quarks are described in the theory using 4 component Dirac spinors. Imposing $SU(N)$ symmetry requires the introduction of $N^2 - 1$ gauge bosons. These are vector particles (spin 1) and mediate interactions between the quarks. In a non-Abelian theory such as QCD, the gluons also interact among themselves. Omitting gauge fixing terms, we can write the Lagrangian density as,

$$\mathcal{L} = \overline{\psi}_i(i\not{D} - m)_{ij}\psi_j - \frac{1}{4}G^a_{\mu\nu}G^{a\mu\nu}. \tag{1.1}$$

The quark fields ψ_i live in the fundamental representation of the gauge group, and carry a colour index i, while the gluon fields are in the adjoint representation. They carry a colour index a which runs from $1 \ldots N^2 - 1$. The slash notation is conventional, and represents contraction with the gamma matrices,

$$\not{D} = D^\mu \gamma_\mu. \tag{1.2}$$

The gamma matrices satisfy the Clifford algebra,

$$\gamma^\mu \gamma^\nu + \gamma^\nu \gamma^\mu = 2g^{\mu\nu}. \tag{1.3}$$

The symbol D^μ_{ij} is the covariant derivative. It is given by

$$D^\mu_{ij} = \partial^\mu \delta_{ij} - igt^a_{ij} A^\mu_a. \tag{1.4}$$

We see that the Lagrangian (1.1) contains the quark-gluon-gluon interaction term. The matrices t^a_{ij} are the generators of the fundamental representation of $SU(N)$. They satisfy commutation relations characteristic of the gauge group,

$$[t^a, t^b] = if^{abc} t^c. \tag{1.5}$$

The second term in Eq. (1.1) describes the kinetic energy of the gluons. It is written in terms of the field strength tensor, defined by

$$[D_\mu, D_\nu] = igt^a G^a_{\mu\nu}, \tag{1.6}$$

where

$$G^a_{\mu\nu} = \partial_\mu A^a_\nu - \partial_\nu A^a_\mu + g f^{abc} A^b_\mu A^c_\nu. \tag{1.7}$$

We see that the kinetic energy part contains not only the expected quadratic piece, describing a true kinetic energy term, but also terms trilinear and quadrilinear in the gluon field. These terms are characteristic of a non-Abelian theory, and indicate that the gauge bosons will interact among themselves.

Scattering amplitudes are related to objects called *correlation functions*, which in turn are obtained from the generating functional of the theory,

$$Z[\eta, \overline{\eta}, J] = \int \mathcal{D}\psi \mathcal{D}\overline{\psi} \mathcal{D}A \exp\left[i \int \mathrm{d}^4x (\mathcal{L} + \eta\overline{\psi} + \overline{\eta}\psi + JA)\right], \tag{1.8}$$

where η, $\overline{\eta}$ and J are source terms for the quark, anti-quark and photon fields respectively. The generating functional Z is a sum over quantum states. Ordinarily this is equivalent to an integral over the space of all field configurations, as written above. However, in the case of gauge theories such as QCD, the same quantum state is represented by an entire subspace of gauge field configurations, and so Eq. (1.8) as written effectively overcounts these states. What is needed is a means of restricting the path integral to physical states, i.e. those not related to each other by a gauge transformation. We can do this by introducing extra terms into the Lagrangian,

$$\mathcal{L} = \mathcal{L}_{classical} - \frac{1}{2\xi}(\partial_\mu A^\mu_a)^2 + (\partial_\mu \chi^*_a)(\partial^\mu \delta_{ab} - g f^{abc} A^\mu_c)\chi_b, \tag{1.9}$$

where we have used the covariant gauge. We have introduced an extra field, called the ghost field, which cancels unphysical polarisation modes of the gluon. The ghost field is unphysical in that it cannot appear in external states, but it does appear as an internal particle inside loop diagrams. For more information on these issues the reader is directed to [1,2].

1.1.1 The Feynman Rules

The physical quantities that we are interested in calculating are typically cross sections describing the scattering of particles, or decay rates. Theoretically, these processes are described by the S matrix. The elements of this matrix describe the amplitudes for scattering (or decay) processes. Unfortunately, calculating these elements is extremely difficult. Normally we are restricted to perturbation theory, in which we expand a given S matrix element as a series in a small parameter. The success of this procedure depends on how small this parameter actually is (as well as the behaviour of the coefficients). In QCD we use the strong coupling α_s, which is related to the coupling g which appears in the Lagrangian by

$$\alpha_s = \frac{g^2}{4\pi}. \tag{1.10}$$

The terms in the perturbative expansion can be evaluated order by order using Feynman diagrams. This is a pictorial method in which we draw all possible diagrams, conforming to a set of rules, which can contribute to a

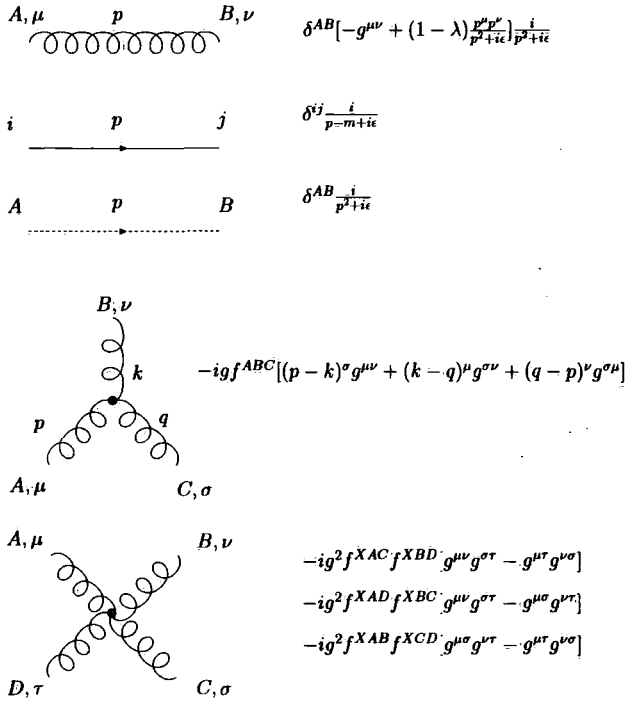

Figure 1.1: Feynman rules in covariant gauge. In the rule for the three gluon vertex all momenta are considered incoming.

certain process at a certain order. The diagrams are then evaluated using the *Feynman rules*. Each piece of the diagram (lines, vertices etc.) are assigned a certain mathematical object. Combining these in the appropriate way gives us the amplitudes we require. Each amplitude will receive contributions from various diagrams. Individual diagrams are not physical objects as they are gauge-dependent, but when they are summed the gauge dependence drops out. The Feynman rules for QCD are illustrated in Fig.(1.1) and Fig.(1.2).

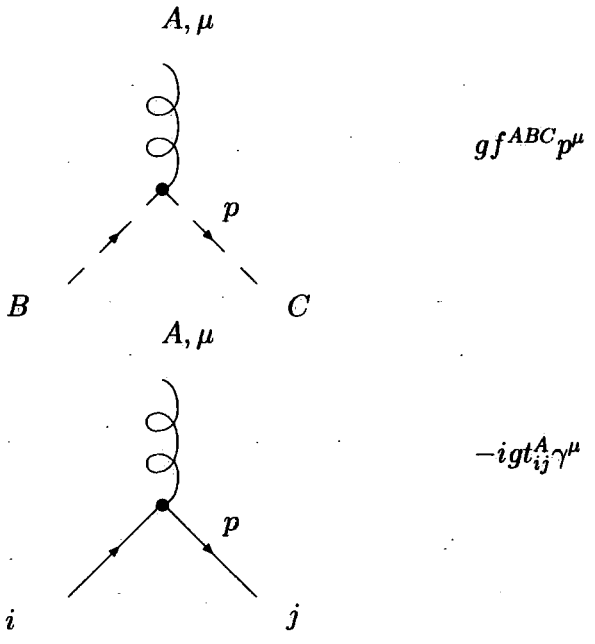

Figure 1.2: Feynman rules in covariant gauge (cont'd)

1.2 Regularisation and Renormalisation

Loop amplitudes in QCD are generally divergent in the ultraviolet. By this we mean that very high energy modes propagate unchecked and lead to infinities in four dimensions. In order to make sense mathematically, the loop integrals must be regulated. This regularisation can be performed in a variety of ways, but by far the most convenient and widely used is dimensional regularisation. In this scheme we perform the integrals in $d = 4 - 2\epsilon$ dimensions. What were infinities in four dimensions now appear as poles in the parameter ϵ. The physically relevant case is of course $\epsilon \to 0$. The presence of the poles in ϵ is not a disaster, provided we admit that QCD is not applicable at very high energies. In these regimes we imagine some form of

overarching unified theory to take over, which must contain QCD (and the rest of the standard model) as a low energy effective theory. The problem we face is that low energy physics appears to receive contributions from high energy phenomena through the loop integrals. However, because QCD is a renormalisable theory, we can still use it to make predictions of low energy physics. This is achieved by a particular parameterisation. We have various free parameters in the Lagrangian, such as the charge g, masses m_i and normalisations of the fields. These bare parameters are unphysical in that they do not in general correspond to quantities measured experimentally. We can organise the theory such that the influence of high energy modes is confined to these parameters, and then define them operationally in terms of real-world measurements. This amounts to taking the high-energy physics from experiment and using QCD to predict the low energy physics.

In practise this means setting the bare parameters to be divergent in such a way as to render all amplitudes UV finite. It is by no means obvious that this is possible - there are only a small number of bare parameters, but a large number of UV divergent amplitudes. The renormalisability of QCD was proven by 't Hooft and Veltman in [3]. We rewrite the bare Lagrangian in terms of renormalised parameters,

$$\mathcal{L}(\{F_i^B\}) = \mathcal{L}(\{F_i\}) + \delta\mathcal{L}(\{F_i\}) \tag{1.11}$$

where F_i denotes any of the free parameters of the Lagrangian. The B su-

perscript indicates that this is a bare quantity. The renormalised parameters F_i are defined multiplicatively. For example, for the gluon field we write

$$A^a_\mu|_{bare} = Z_3^{1/2} A^a_\mu|_{ren}. \tag{1.12}$$

We can calculate Z_3 order by order in perturbation theory. It will be divergent, that is to say, it will contain poles in the dimensional regularisation parameter ϵ. These poles will cancel some of the poles arising from the loop integrals. The quark field is renormalised with a factor Z_2,

$$\psi|_{bare} = Z_2^{1/2} \psi|_{ren}, \tag{1.13}$$

and similarly for all the parameters in the Lagrangian. Once renormalisation has been carried out, we find extra Feynman rules correcting the vertices and propagators. The contribution of the extra diagrams cancels the UV divergent parts of the original set of diagrams.

1.2.1 The Running Coupling

When we use dimensional regularisation, we are forced to introduce a dimensionful coupling $g\mu^\epsilon$ so that the action remains dimensionless. The parameter μ is arbitrary, so physical quantities cannot depend on it. Once the divergences are subtracted, the finite parts of the amplitudes retain a dependence on μ, and so does the coupling $g = g(\mu)$. Predictions of a physical observable

$\mathcal{O}$ therefore take the schematic form

$$\mathcal{O} = \sum_{n=n_0} C_n(\mu)\ \alpha_s^n(\mu). \tag{1.14}$$

We see that both the coupling and the coefficients of the perturbative expansion depend on the unphysical scale μ. This dependence cancels when they are combined as in (1.14). Unfortunately, it is beyond our abilities to calculate more than a few terms of this series, and so we must truncate it at some order m. Our prediction $\mathcal{O}_m$ will then suffer from a residual renormalisation scale dependence. One of the advantages of calculating higher order corrections is the partial elimation of this unphysical dependence. In practise we choose μ to be equal to one of the typical scales in the process under consideration, in an effort to keep logarithms of the form

$$\ln \frac{\mu^2}{s_{ij}}, \tag{1.15}$$

where $s_{ij} = 2\ p_i \cdot p_j$ is the Lorentz invariant product of two of the external momenta, as small as possible. As we have described, the QCD coupling α_s is a function of the renormalisation scale μ. This dependence on an unphysical scale is a result of the way in which we have shifted contributions of high-energy modes out of the Feynman diagrams and into the coupling. The

precise functional form of α_s is governed by the beta function,

$$\mu^2 \frac{\partial \alpha_s}{\partial \mu^2} = \beta(\alpha_s). \tag{1.16}$$

The beta function can be calculated in perturbation theory. It is expanded in powers of the coupling,

$$\beta(\alpha_s) = -\beta_0 \alpha_s^2 - \beta_1 \alpha_s^3. \tag{1.17}$$

If we retain only the first term in the perturbative expansion of the beta function, we can solve (1.16). We find

$$\alpha_s(\mu^2) = \frac{\alpha_s(\mu_0^2)}{1 + \alpha_s(\mu_0^2)\ \beta_0\ \ln(\mu^2/\mu_0^2)}. \tag{1.18}$$

This equation gives the running of the strong coupling. Given α_s at a scale μ_0, we can evaluate it at any other scale μ. Experimental quotes of the coupling must specify a scale. It has become customary to use the Z mass for this purpose. At the time of writing the world average experimental value is [4]

$$\alpha_s(M_Z) = 0.1176 \pm 0.002. \tag{1.19}$$

1.3 Cross Sections at NLO

Although the underlying $SU(N_c)$ gauge theory is well understood, accurately predicting the results of experiments involving quarks and gluons is far from trivial. In this section we will outline the basic procedure. Suppose we are interested in the cross section for two initial state partons to produce m final state partons. This cross section can be written

$$\sigma = \sigma_{LO} + \sigma_{NLO}, \tag{1.20}$$

where we have separated the contributions according to the power of α_s. The leading order (LO) contribution is obtained by integrating the Born amplitude squared over the available phase space,

$$\sigma_{LO} = \frac{1}{2s} \int |M|^2 \, F^{(m)} \, d\Gamma. \tag{1.21}$$

Here we have introduced the *measurement function* $F^{(m)}$, which defines the experimental observable under consideration. To ensure infrared safety, we require that when an $m+1$ parton configuration becomes degenerate with an m parton configuration, as for instance when a soft or collinear parton is emitted, the measurement function behaves similarly, i.e.

$$F^{(m+1)} \to F^{m}. \tag{1.22}$$

This allows the cancellation of soft and collinear singularities, in accordance with the KLN [5, 6] theorem. Because Born level amplitudes are relatively easy to obtain, if not analytically then via numerical routines such as MADGRAPH [7], the Born level cross section poses few problems. In practise the integral is impossible to perform analytically, but can be easily evaluated using Monte Carlo numerical integration.

At next-to-leading order (NLO) we must consider two contributions to σ_{NLO}

- the real contribution σ^R, obtained from final states with $m+1$ partons
- the virtual contribution σ^V, obtained from final states with m partons.

Note that these quantities are not by themselves physically well defined. They are each afflicted by infrared singularities caused by soft and collinear partons. The total NLO cross section is obtained from a sum of these two contributions,

$$\begin{aligned} \sigma_{NLO} &= \sigma^R + \sigma^V \\ &= \int_{m+1} d\sigma^R + \int_m d\sigma^V \\ &= \frac{1}{2s}\int_{m+1} |M^{m+1}|^2 F^{(m+1)}\, d\Gamma_{m+1} + \frac{1}{2s}\int_m |M_m^{1-loop}|^2 F^{(m)}\, d\Gamma_m \end{aligned} \tag{1.23}$$

The IR singularities appear directly in $|M_m^{1-loop}|^2$ as poles in ϵ. They arise from evaluating the (dimensionally regulated) loop integrals. These poles will be cancelled by similar poles in the real contribution, which appear

after the integral has been performed. Thus we see that bringing about the cancellation of ϵ poles and integrating the finite remainder requires a combination of analytic and numerical methods.

1.4 The Helicity Method

In this thesis we will be interested in polarised scattering cross sections, and so we will need to calculate helicity sub-amplitudes. In fact, even for processes where we intend to sum over all spins, it is often a great simplification to consider first the separate helicity amplitudes, and then sum over these numerically. For helicity amplitudes the kinematical invariants such as dot products $p_i \cdot p_j$ are not the most suitable variables. Instead, they find their simplest expression in terms of spinor products. In this section we outline the basic formalism behind these objects, and describe how they can be numerically evaluated.

It was discovered long ago [8–13] that amplitudes involving massless momenta p_i and p_j can be conveniently represented in terms of spinor products defined as,

$$[ij] = \bar{u}^+(p_i)u^-(p_j) \quad \text{and} \quad \langle ij \rangle = \bar{u}^-(p_i)u^+(p_j). \tag{1.24}$$

In this way amplitudes find their simplest expression. The spinors in question can be thought of either as two-component Weyl or 4-component Dirac

spinors. Numerical evaluation of such amplitudes involves the use of the standard formulae for the spinor products in terms of the momentum 4-vectors. Following [14], let us first introduce two 4-vectors k_0 and k_1 such that

$$k_0 \cdot k_0 = 0 \ , \ k_1 \cdot k_1 = -1 \ , \ k_0 \cdot k_1 = 0. \tag{1.25}$$

We now define a basic spinor $u^-(k_0)$ via

$$u^-(k_0)\bar{u}^-(k_0) = \frac{1-\gamma^5}{2}\not{k}_0, \tag{1.26}$$

and choose the corresponding positive helicity state to be

$$u^+(k_0) = \not{k}_1 u^-(k_0). \tag{1.27}$$

Using these definitions it is possible to construct spinors for any null momentum p as follows:

$$u^\lambda(p) = \frac{\not{p}\, u^{-\lambda}(k_0)}{\sqrt{2p \cdot k_0}}, \tag{1.28}$$

with $\lambda = \pm$. Note that this satisfies the massless Dirac equation $\not{p}u(p) = 0$,

as required. We can now simply evaluate spinor products. For example,

$$
\begin{aligned}
[ij] &= \bar{u}^+(p_i)u^-(p_j) && (1.29)\\
&= \frac{\bar{u}^-(k_0)\ \not{p}_i\ \not{p}_j\ u^+(k_0)}{\sqrt{4\ (p_i\cdot k_0)(p_j\cdot k_0)}} && (1.30)\\
&= \frac{\mathrm{Tr}(\frac{(1-\gamma^5)}{2}\ \not{k}_0\ \not{p}_i\ \not{p}_j\ \not{k}_1)}{\sqrt{4\ (p_i\cdot k_0)(p_j\cdot k_0)}} && (1.31)\\
&= \frac{(p_i\cdot k_0)(p_j\cdot k_1)-(p_j\cdot k_0)(p_i\cdot k_1)-i\epsilon_{\mu\nu\rho\sigma}k_0^\mu p_i^\nu p_j^\rho k_1^\sigma}{\sqrt{(p_i\cdot k_0)(p_j\cdot k_0)}}. && (1.32)
\end{aligned}
$$

The angle bracket product is related[1] to the square bracket product by complex conjugation and a sign, i.e. $\langle ij\rangle = -[ij]^*$. The arbitrary k_0 and k_1 can now be chosen so as to yield as simple an expression for the product $[ij]$ and $\langle ij\rangle$ as possible, to facilitate numerical evaluation of the ampitudes. The choice[2]

$$k_0 = (1,0,0,1) \tag{1.33}$$

$$k_1 = (0,0,1,0) \tag{1.34}$$

is a good one, giving the familiar

$$[ij] = (p_i^y + ip_i^x)\left[\frac{p_j^0-p_j^z}{p_i^0-p_i^z}\right]^{\frac{1}{2}} - (p_j^y+ip_j^x)\left[\frac{p_i^0-p_i^z}{p_j^0-p_j^z}\right]^{\frac{1}{2}}. \tag{1.35}$$

In the course of evaluating a Feynman diagram we will also encounter polar-

[1]The reader should note that a similar definition with the opposite sign is found in some of the literature.

[2]The notation is $k^\mu = (k^0, \mathbf{k})$.

isation vectors. These are the external wavefunctions of gauge bosons such as gluons. In this thesis we will only be concerned with the massless external gauge bosons (gluon, photon), and not the massive weak gauge bosons $W^{\pm}$ and Z. Consequently we can restrict ourselves to $\epsilon(p)$ where $p^2 = 0$. We can write this in terms of spinors by introducing an auxiliary vector k for each external gauge boson. In some sense this parameterises the gauge, and so the final answers we obtain for gauge invariant quantities such as a partial amplitude must be independent of k. In practise, we usually set k to be one of the external momenta, though we are not allowed to set it parallel to its associated p. There are different expressions depending on the helicity of the boson,

$$\epsilon_{\mu}^{+}(p,k) = \frac{\bar{u}^{-}(k)\,\gamma_{\mu}\,u^{-}(p)}{\sqrt{2}\,\langle kp\rangle}, \tag{1.36}$$

$$\epsilon_{\mu}^{-}(p,k) = \frac{\bar{u}^{+}(k)\,\gamma_{\mu}\,u^{+}(p)}{\sqrt{2}\,[pk]}. \tag{1.37}$$

Note that there are only two physical polarisations. It is also useful to have at hand the 'slashed' form

$$\not{\epsilon}^{+}(p,k) = \sqrt{2}\,\frac{u_{+}(k)\bar{u}_{+}(p) + u_{-}(p)\bar{u}_{-}(k)}{\langle kp\rangle}, \tag{1.38}$$

$$\not{\epsilon}^{-}(p,k) = \sqrt{2}\,\frac{u_{+}(p)\bar{u}_{+}(k) + u_{-}(k)\bar{u}_{-}(p)}{[pk]}. \tag{1.39}$$

Recall that Dirac-slashing refers to contraction with a gamma matrix, so that for a four vector A^{μ} we have $\not{A} = A^{\mu}\gamma_{\mu}$.

1.4.1 Massive spinors

For processes involving the light quarks u,d,s and to some extent also the charm c, it is a good enough approximation to set the quark mass to zero. This is because for the high energy processes with which we typically concern ourselves, these quark masses are dwarfed by the high centre of mass energies involved. For bottom quarks this approximation starts to look a little suspect, and for the top it is clearly not valid at all. So, it is important for us to be able to handle the corresponding massive spinors. To evaluate spinor products involving massive spinors, we need to find a definition analogous to (1.28). One possibility is that outlined in [14],

$$u^{\lambda}(p) = \frac{(\not{p} + m)u^{-\lambda}(k_0)}{\sqrt{2p \cdot k_0}}, \tag{1.40}$$

which satisfies the massive Dirac equation, $(\not{p} - m)u^{\lambda}(p) = 0$. The m in (1.40) is positive or negative when $u^{\lambda}(p)$ describes a particle or antiparticle respectively. This definition has the virtue[3] of being smooth in the limit $m \to 0$. We will use (1.40) to evaluate products involving massive spinors.

It is easily seen that the familiar $[.\ .]$ and $\langle .\ . \rangle$ products take the same form for massive spinors as they do for massless ones. Explicit mass terms drop out due to various trace theorems. However, the product of like-helicity

[3]Care is needed when $p \cdot k_0$ also vanishes in this limit, as we will discuss later.

spinors is now non-zero:

$$\begin{aligned}(ij) &= \bar{u}^{\pm}(p_i)u^{\pm}(p_j), && (1.41)\\ &= m_i\left(\frac{p_j\cdot k_0}{p_i\cdot k_0}\right)^{\frac{1}{2}} + i \leftrightarrow j && (1.42)\\ &= m_i\left(\frac{p_j^0 - p_j^z}{p_i^0 - p_i^z}\right)^{\frac{1}{2}} + i \leftrightarrow j, && (1.43)\end{aligned}$$

where in the last line we have used k_0 as given in (1.33). Note that the like-helicity product is the same whatever the helicity of the spinors involved, and that we use a round bracket as a shorthand notation for it.

We have been using the word 'helicity' to refer to the spin projection of massive fermions, but in fact this is only justified if the projection is onto the direction of the momentum vector. For massive particles it is not obvious that this is the case. However, one can define a unique polarisation vector, that defines the direction along which we are projecting the particle's spin,

$$\sigma^\mu = \frac{1}{m}\left(p^\mu - \frac{m^2}{p\cdot k_0}k_0^\mu\right). \tag{1.44}$$

This vector depends on an arbitrary reference momentum k_0. The spinors (1.40) satisfy

$$(1 - \lambda\gamma^5\not{\sigma})u^\lambda = 0. \tag{1.45}$$

We see that besides the momentum p there is an additional contribution to the polarization vector proportional to k_0. Suppose we have an anti-fermion

i and fermion j in the initial state and they approach along the z axis, in the positive and negative directions respectively. If we choose k_0 to be a unit vector in the z direction, i.e.

$$k_0 = (1,0,0,1), \tag{1.46}$$

then for momenta[4]

$$p_i = (E,0,0,\beta E), \tag{1.47}$$

$$p_j = (E,0,0,-\beta E), \tag{1.48}$$

we have the following polarization vectors:

$$\sigma_i^\mu = \frac{1}{m_i}(-E\beta,0,0,-E), \tag{1.49}$$

$$\sigma_j^\mu = \frac{1}{m_j}(E\beta,0,0,-E). \tag{1.50}$$

If we recall that m_i is negative because i is an antiparticle, then we see that each polarization vector points in the same direction as the corresponding momentum, so that the spinors $u^\lambda(p)$ are indeed helicity eigenstates for this choice of k_0. However, choosing k_0 to be parallel to one of the particle's momenta results, in the massless limit, in the denominators of products such as that in (1.43) vanishing. By being careful to take the limit algebraically

[4] $\beta = (1 - \frac{m^2}{E^2})^{1/2}$

this does not present a problem.[5] But it should be noted that in such cases products like (ij) do not necessarily vanish in the massless limit. We can sidestep this issue by choosing a different k_0, though we could not then talk of the helicity of the fermion.

Useful Spinor Product Identities

We summarise here some of the identities which have proven useful during the course of our calculations involving massive spinor products. Firstly, the ubiquitous expression $\bar{u}^{\pm}(i) \not{p} u^{\pm}(j)$ can be handled by using the well known formula

$$\begin{aligned} \not{p} - m &= \sum u_\lambda(p)\, \overline{u}_\lambda(p) \\ &= u_+(p)\, \overline{u}_+(p) + u_-(p)\, \overline{u}_-(p), \end{aligned}$$

which give us

$$\begin{aligned} \bar{u}^+(i) \not{p} u^+(j) &= [ip]\langle pj\rangle + (ip)(pj) + m(ij), \\ \bar{u}^-(i) \not{p} u^-(j) &= \langle ip\rangle[pj] + (ip)(pj) + m(ij), \\ \bar{u}^+(i) \not{p} u^-(j) &= (ip)[pj] + [ip](pj) + m[ij], \\ \bar{u}^-(i) \not{p} u^+(j) &= \langle ip\rangle(pj) + (ip)\langle pj\rangle + m\langle ij\rangle. \end{aligned}$$

[5] If we take $k_0^\mu = (1, 0, \sin\theta, \cos\theta)$, then for the momenta defined in (1.47) and (1.48), with $m_j = -m_i = m$, we have $(ij) = -2m\beta\cos\theta(1-\beta^2\cos^2\theta)^{-1/2}$. Thus $(ij) \sim O(m)$ as $m \to 0$ except if $\theta = 0°$ when $(ij) \sim O(E)$.

Whereas for massless vectors k_i,k_j we have the familiar relation $2k_i \cdot k_j = \langle ij\rangle[ji]$, in the massive case this is extended to

$$2p_i \cdot p_j = \langle ij\rangle[ji] + (ij)^2 - 2m_i m_j. \tag{1.51}$$

For any massive i,j and massless k, l we have

$$\begin{aligned} (ik)(jl) &= (il)(jk), & (1.52)\\ (ik)[li] + [ik](li) &= m_i[lk], & (1.53)\\ \bar{u}^{\pm}(p_k)\, \not{p}_i\, u^{\mp}(p_l) &= 0 & (1.54) \end{aligned}$$

Another useful formula is the Schouten identity,

$$\langle a\ b\rangle\langle c\ d\rangle + \langle a\ c\rangle\langle d\ b\rangle + \langle a\ d\rangle\langle b\ c\rangle = 0. \tag{1.55}$$

1.5 Colour Ordering

Even if one is interested primarily in spin-summed cross sections, it is useful to evaluate the individual helicity amplitudes separately. Amplitudes typically find their most compact expression in this way, expressed in terms of spinor products. If one wants to sum over all spins then this can be done numerically at the end of the calculation. In fact, since in this thesis we are interested in a polarised scattering process, we are obliged to use helicity amplitudes. The way we treat the colour structure of QCD processes is similar

to this. The amplitudes can be expressed as a series of colour structures, with gauge-independent coefficients. The coefficients are called partial sub-amplitudes. Recall that the colour factors for each Feynman diagram come from various t^a matrices etc. originating in the Feynman rules. For example, for the $2 \to 2$ scattering process $gg \to b\bar{b}$ there are only three contributing colour structures, namely

$$C_1 = (t^A\, t^B)_{ij}, \qquad C_2 = (t^B\, t^A)_{ij}, \qquad C_3 = \delta^{AB}\delta_{ij}. \tag{1.56}$$

In fact the third structure C_3 does not contribute at tree level. Other processes will be expanded in a different basis of colour structures. By defining a modified set of Feynman rules, given in e.g. [15], in which there are no colour dependent factors, and restricting the set of diagrams considered, we can evaluate directly any of the partial sub-amplitudes. In particular, we only consider diagrams with a particular *ordering* of the external partons. The partial amplitudes are then evaluated separately, one for each ordering. When we come to square the amplitude, the partial amplitudes are multiplied numerically, and we evaluate the colour factors by hand.

So, by colour ordering we mean the separation of kinematic and group theoretical factors. The price of this separation is that we now need to evaluate various *partial amplitudes*, which are the kinematic coefficients of the colour structures. Each partial amplitude is distinguished by a particular ordering of the external partons and only those Feynman diagrams with the

requisite parton ordering (and hence colour structure) contribute to a given partial amplitude. Each partial amplitude is gauge independent, and as such can be worked out in isolation to others. In this way we break up the problem into smaller pieces. This is why the colour decomposition is so useful.

Apart from the example above, the other process we will be concerned with in this thesis is $gg \to b\bar{b}g$. Because there are more partons involved, there are more colour structures that can contribute. It is not difficult to see that the only structures present are of the form,

$$(t^A t^B t^C)_{ij}, \tag{1.57}$$

for some ordering of $\{A, B, C\}$. There are therefore $3! = 6$ different structures. Of course, the three-gluon vertices will contribute factors of f^{ABC}, but these can always be re-written using the commutation relation,

$$[t^A, t^B] = i f^{ABC} t^C. \tag{1.58}$$

1.6 Outline of this Thesis

In the two chapters which follow this introduction, we describe alternatives to the usual Feynman diagram method of evaluating gauge theory amplitudes. These new techniques are inspired by a correspondence [16] due to Witten between the superymmetric gauge theories and a certain string theory defined in Twistor space. These new methods are distinguished by their

use of on-shell building blocks, and thus avoid much of the computational difficulty associated with Feynman diagrams, which use gauge-dependent, off-shell quantities in intermediate steps. In Chapter 2 we will discuss the applicability of these new methods to a simpler gauge theory - QED. The on-shell techniques were originally envisioned as only applying to massless partons. Gradually after their introduction it was found [17,18] how they can be used for amplitudes with massive fermions, thus increasing still further their appeal to phenomenologists. In Chapter 3 we explain one way in which such massive partons can be accomodated.

In Chapter 4 we outline the calculation of the loop corrections to the process $gg \to b\bar{b}$. We maintain full generality, that is we keep all the spin and colour information. This calculation is a necessary input to any NLO analysis of the central exclusive production of dijet final states. In Chapter 5 we describe in some detail the phenomenological appeal of this production mechanism, and the relevance of the amplitudes presented in this thesis.

Chapter 2

QED Amplitudes from Twistor Space

2.1 Introduction

The calculation of cross sections for multi-particle scattering processes is restricted primarily by the technical difficulties associated with the evaluation of the corresponding amplitudes. These difficulties are due to the factorial growth in the number of diagrams as the number of external particles is increased. Also, the number of terms in the expression for each diagram quickly increases. Significant progress was made in 2004 when Witten [16] discovered a connection between gauge field theories in four dimensions and a string theory defined on twistor space. It was found that field theory amplitudes, when re-expressed in terms of twistor space variables, exhibited a

structure that was not previously apparent. This development was interesting from a theoretical point of view, because it suggested hitherto unknown mathematical structure in familiar gauge field theories. It may be hoped that such a reformulation will be the springboard for further progress. As well as this, there was considerable interest among phenomenologists in the promise of improved calculational methods, for this work suggested much improved techniques for the calculation of tree level amplitudes. These new techniques permitted analytical expressions to be worked out for the first time for amplitudes with up to eight external particles. It also led to much more compact forms for known amplitudes, which is important for practical applications - the less time required for each function call the higher statistics can be obtained in a numerical integration routine such as Monte Carlo.

The correspondence that Witten discovered applied only to purely gluonic $\mathcal{N} = 4$ supersymmetric Yang-Mills theory at tree level. However, at tree level the amplitudes of this theory coincide with those of QCD. This is easily understood when one considers that the absence of loops means that in purely gluonic diagrams there can be no involvement of the other fields in the SUSY multiplet. This made the correspondence a useful phenomenological tool. Gradually, the scope was extended - for example they were shown to be useful also for amplitudes involving quarks [18, 19]. In this chapter we will describe the application of the so-called 'MHV-rules' and BCF recursion relations (these terms will be explained in the proper place) to QED amplitudes. We will begin by describing what MHV amplitudes are and how they

are incorporated in a scalar perturbation theory. We will illustrate our findings with numerous examples of increasing complexity, checking the results against an old, yet impressively concise, formulation in terms of Feynman diagrams.

2.1.1 MHV amplitudes

Let us consider colour ordered amplitudes at tree level involving only gluons. Parke and Taylor [20] conjectured that these take remarkably simple forms depending on the helicities of the external partons. This was later proven using a recursive technique by Berends and Giele [21]. When all the helicities are positive[1], or if only one is negative, then the amplitude vanishes,

$$A(1^+, 2^+, ..., n^+) = 0, \tag{2.1}$$

$$A(1^+, 2^+, ..., i^-, ..., n^+) = 0. \tag{2.2}$$

These amplitudes are colour ordered partial amplitudes - see Chapter 1 for an explanation of this. In this chapter we adopt the convention that all particles are incoming, so that momentum conservation reads $\sum_{i=1}^{n} p_i = 0$. When two of the partons have negative helicity, and the rest positive, the amplitude is

[1]We will consider only amplitudes with a majority of positive helicity partons. The remaining configurations are obtained by parity invariance.

no longer zero. It is, however, only one term [20, 21],

$$A(1^+, 2^+, ..., i^-, ..., j^-, ..., n^+) = \frac{\langle i\ j\rangle^4}{\prod_{k=1}^{n}\langle k\ k+1\rangle}. \tag{2.3}$$

This type of helicity configuration is described as being maximally helicity violating (MHV). These results are valid *for all n.* This represents a large scale cancellation of terms in a Feynman diagram expansion. Consider that for high n many millions of terms are cancelling down to a single term. This structure is in no way obvious at the level of the Lagrangian. Increasing beyond two the number of negative helicity particles leads to more complicated expressions, but nonetheless, the simplicity of these results is impressive.

2.2 Kleiss-Stirling approach to $e^+e^- \rightarrow n\gamma$

Let us digress now to consider an old result. Consider the process

$$e^-(p_a) + e^+(p_b) \rightarrow \gamma(k_1) + \gamma(k_2) + ... + \gamma(k_n) \tag{2.4}$$

In the massless (electron) limit, helicity is conserved at each fermion-photon vertex and so the helicities of the electron and positron will be opposite, $h_{e^-} = -h_{e^+}$. There are therefore 2^{n+1} distinct spin amplitudes (two polarisations for each photon and $h_{e^-} = \pm$). In the traditional approach, the $(n!)$ Feynman diagrams are obtained simply by joining the n photons to the fermion line in all possible ways. Labelling the distinct polarisation states by $S = 1, ..., 2^{n+1}$

gives an expression for the unpolarised cross section of

$$d\sigma_n = \frac{1}{F}\,[d\Phi_n]\,\frac{1}{n!}\,\frac{1}{4}\sum_S |M_S|^2 \tag{2.5}$$

where the terms on the right-hand side are the flux factor, the phase space volume element, the symmetry factor and the spin-summed/averaged amplitude squared respectively.

The KS result is[2] [14]

$$\begin{aligned} M_S = & \left(\prod_{j=1}^{n} p\cdot k_j\right)^{-1/2} \sum_{D=1}^{n!} \langle p_a\, a_1\rangle\,[p_b\, b_n] \\ & \times \prod_{i=1}^{n-1}\left\{\frac{\langle \hat{q}_i\, a_{i+1}\rangle\,[\hat{q}_i\, b_i]}{q_i^2} + \frac{\langle p\, a_{i+1}\rangle\,[p\, b_i]}{2p\cdot q_i}\right\} \end{aligned} \tag{2.6}$$

where p^μ is an arbitrary light-like four vector and

$$\begin{aligned} a_i = p,\ b_i = k_i \quad &\text{if} \quad h_i = +\,, \\ a_i = k_i,\ b_i = p \quad &\text{if} \quad h_i = -\,. \end{aligned} \tag{2.7}$$

The sum in (2.6) is over the $n!$ distinct permutations $\hat{k}_1, \hat{k}_2, \ldots$ of the photon

[2]This expression corresponds to the choice $h_{e^-} = -$. The corresponding $h_{e^-} = +$ amplitudes are readily obtained using parity invariance.

momenta $k_1, k_2, ...$, from which internal four-momenta are defined by

$$\begin{aligned} q_i &= \sum_{j=1}^{i} \hat{k}_j - p_a \,, \quad i = 1, ..., n \quad (q_n \equiv p_b) \,, \\ \hat{q}_i &= q_i - \frac{q_i^2}{2p \cdot q_i} p_i \,, \quad (\hat{q}_i^2 = 0) \,. \end{aligned} \tag{2.8}$$

The $\langle ij \rangle$ and $[ij]$ spinor products that appear in Eq. (2.6) are defined in the introduction. The full expression for the amplitude for arbitrary n can then be written in just a few lines of computer code. Note that the result for the amplitude squared is independent of p^μ (which is related to the choice of photon gauge) and this provides a powerful check on the calculational procedure.

2.2.1 Photons

The main difference when we consider QED is that there are no pure-photon tree-level amplitudes, because photons do not self-interact. There must always be (at least) one pair of fermions present, which (if massless) must be of opposite helicity due to our convention that all particles are incoming. Also, in contrast to non-Abelian theories there is no concept of colour ordering, so we will be concerned with full physical amplitudes rather than colour-ordered partial amplitudes. It is again the case that amplitudes with only one negative helicity particle (which must be either the fermion or anti-fermion – we

shall take it to be the former) vanish,

$$A^{\rm QED}(\overline{f}^+, f^-, 1^+, 2^+, ..., I^+, ..., n^+) = 0\,. \tag{2.9}$$

Here I^+ denotes a positive helicity photon with momentum p_i, and f, $\overline{f}$ denote fermion and anti-fermion respectively. The dots in Eq. (2.9) indicate positive helicity photons. The MHV amplitudes, which are those with two negative helicity particles, take the following form (for massless fermions):

$$A^{QED}(\overline{f}^+, f^-, 1^+, 2^+..., I^-, ..., n^+) = \frac{2^{\frac{n}{2}} e^n \langle f\overline{f}\rangle^{n-2}\langle fI\rangle^3\langle \overline{f}I\rangle}{\prod_{k=1}^n \langle fk\rangle\langle \overline{f}k\rangle}. \tag{2.10}$$

This is the fundamental MHV amplitude in QED, and as before it consists of only a single term. The factor e^n is the gauge coupling constant, which we will normally omit in what follows. It is possible [13] to obtain the amplitude in (2.10) by symmetrizing colour-ordered non-Abelian amplitudes,

$$A^{QED}(\overline{f}, f, 1, 2, 3, ..., n) = A(\overline{f}, f, 1, 2, 3, ..., n) + A(\overline{f}, f, 2, 1, 3, ..., n) + ... \,. \tag{2.11}$$

Each term on the right-hand side is a colour-ordered MHV (Parke-Taylor) QCD amplitude, and we sum over $n!$ permutations of n gluons. A factor of $2^{\frac{n}{2}}$ must also be included to take account of different generator normalizations – our QED generators are normalized to unity. It should be noted that in writing (2.10) in this particular way we have made an apparently arbitrary choice of phase. Since the phase of a full (i.e. not partial) amplitude is

not a physical observable, any of the $\langle..\rangle$ products in (2.10) could, naively, be replaced with the corresponding $[..]$ product. We will come back to this point later. It is worth mentioning that due to parity invariance the amplitude with all the helicities flipped has the same magnitude as (2.10) above. Also, one can use charge conjugation invariance to switch the fermion and anti-fermion.

We can write (2.10) in a physically more illuminating way, emphasizing the pole structure:

$$\begin{aligned} A(\overline{f}^+, f^-, 1^+, 2^+ ..., I^-, ..., n^+) &= \frac{\langle fI\rangle^3\langle \overline{f}I\rangle}{\langle f\overline{f}\rangle^2}\prod_{k=1}^{n}\frac{e\sqrt{2}\langle f\overline{f}\rangle}{\langle fk\rangle\langle \overline{f}k\rangle} \\ &= \frac{\langle fI\rangle^3\langle \overline{f}I\rangle}{\langle f\overline{f}\rangle^2}\prod_{k=1}^{n} S_k \,. \end{aligned} \tag{2.12}$$

It is a fundamental result of general quantum field theories that scattering amplitudes have a universal behaviour in the soft gauge boson limit. When all components of a particular photon's momentum are taken to zero, the amplitude factorizes into the amplitude in the absence of that photon multiplied by an 'eikonal factor',

$$S_k = \frac{e\sqrt{2}\langle f\overline{f}\rangle}{\langle fk\rangle\langle \overline{f}k\rangle} \,. \tag{2.13}$$

The form of this factor is universal, by which we mean that any QED amplitude (not only MHV ones) will have a similar behaviour in the soft limit, with the same form for the eikonal factor. Since the QED MHV amplitude is just a single term, it follows that the eikonal factors must be present as factors – and indeed they are.

2.3 The MHV Rules

There has been much recent progress in calculating scattering amplitudes in perturbative Yang-Mills theory. Cachazo, Svrcek and Witten [22] introduced a novel diagrammatic technique, known as the 'MHV rules', in which maximally helicity violating (MHV) amplitudes are used as vertices in a scalar perturbation theory. These vertices are connected by scalar propagators $1/p^2$. This arrangement vastly reduces the number of diagrams that must be evaluated relative to the traditional Feynman rules case. It also means that each diagram requires much less effort to evaluate than with Feynman rules, due mainly to the absence of complicated multi-gluon vertices.

Although the original CSW paper dealt only with purely gluonic amplitudes, the formalism has since then been successfully extended to include quarks [18, 19], Higgs [23, 24] and massive gauge bosons [25]. In this chapter we will use the amplitudes shown in Eq. (2.10) as building blocks, and thereby apply the MHV rules to QED processes. We will derive relatively simple formulae for three, four and five photon amplitudes (an electron and positron are understood to be present also). We first pause to describe in more detail the Weyl spinors and bispinor representation of external momenta that we will use.

The Lorentz group consists of rotations and boosts. Physical theories must be invariant under Lorentz transformations, which means that the fundamental objects we use to describe physical systems must transform in well-

defined ways under the group. The generators of rotations $\mathbf{J}$ and boosts $\mathbf{B}$ do not commute with each other, but one can show that the following combinations do commute:

$$\begin{aligned} \mathbf{M} &= \mathbf{J} + i\mathbf{B}, \\ \mathbf{N} &= \mathbf{J} - i\mathbf{B}, \end{aligned} \tag{2.14}$$

and that, furthermore, $\mathbf{M}$ and $\mathbf{N}$ obey the $SU(2)$ algebra. This means that the Lorentz group is equivalent to two copies of $SU(2)$. Representations of the former can thus be characterised as $m \otimes n$, where m and n label the representations of each of the $SU(2)$ sub-groups. We call objects living in the $\frac{1}{2} \otimes 0$ representation left-handed Weyl spinors. They carry one index only as they are singlets under the second $SU(2)$. Similarly, right-handed Weyl spinors live in the $0 \otimes \frac{1}{2}$ representation. They also carry one index, though it refers to a different representation space and is commonly dotted to emphasise this. The vector representation is $\frac{1}{2} \otimes \frac{1}{2}$, and objects transforming under it carry two indices, one dotted and one undotted. It is more common to write vectors with a single index as follows,

$$p_{a\dot{a}} = \sigma^{\mu}_{a\dot{a}}\, p_{\mu}, \tag{2.15}$$

where $\sigma^{\mu}_{a\dot{a}}$ are the chiral gamma matrices. One can show that massless vectors

can be written using two Weyl spinors,

$$p_{a\dot{a}} = \lambda_a \widetilde{\lambda}_{\dot{a}}, \tag{2.16}$$

so that each massless external leg of an amplitude can be thought of as a pair of Weyl spinors, of opposite chirality[3].

In order to use MHV amplitudes as vertices, it is necessary to continue them off-shell, since internal momenta will not be light-like. We need to define spinors λ for the internal lines. The convention established in [22], which we shall follow, defines λ to be

$$\lambda_a = p_{a\dot{a}} \eta^{\dot{a}} \tag{2.17}$$

for an internal line of momentum $p_{a\dot{a}}$, where $\eta^{\dot{a}}$ is arbitrary. The same η must be used for all internal lines and in all diagrams contributing to a particular amplitude. In practice, it proves convenient to choose η to be one of the conjugate (opposite chirality) spinors $\widetilde{\lambda}$ of the external fermion legs. Note that for external lines, which remain on-shell, λ is defined in the usual way.

Having defined the MHV amplitudes, and the manner in which they are to be continued off-shell, we are now in a position to calculate non-MHV amplitudes. These are simply those with more than two negative-helicity particles.

[3]Left handed spinors have chirality +1 and right handed spinors have chirality -1, though the opposite convention can be found in the literature.

2.3.1 Simple Examples

As a first example let us calculate $A(\overline{f_1^+}, f_2^-, 3^-, 4^-)$.[4] This is expected to vanish, see (2.9). There are two contributing MHV diagrams, though they differ only by a permutation of photons. Note that the external legs are not constrained to be positioned cyclically as in the case of colour-ordered partial amplitudes. The absence of a pure-photon vertex means that the internal lines of MHV diagrams for QED processes with two fermions can only be fermionic. Consider Figure 2.1, which shows the first of the two diagrams. We assign the internal helicities in such a way that each vertex has two negative helicity lines, with the remainder positive. They are then MHV amplitudes. Schematically, the contribution of this diagram is

$$\text{Left Vertex} \times \text{Propagator} \times \text{Right vertex.} \tag{2.18}$$

Taking expressions for the vertices from Eq. (2.10), and using $1/q^2$ for the propagator, the contribution of the diagram in Figure 2.1 can be written down immediately as

$$\sqrt{2}\frac{\langle \lambda_q\, 4\rangle^2}{\langle \lambda_q\, 1\rangle}\frac{1}{q^2}\sqrt{2}\frac{\langle 2\, 3\rangle^2}{\langle 2\, \lambda_q\rangle}\,, \tag{2.19}$$

where λ_q is the spinor representing the internal line of momentum q. This expression is simply a product of two MHV vertices and a propagator. Using

[4]Note the change in notation – the spinor representing the fermion is now denoted 2 (not f) and the spinor representing the anti-fermion is now denoted 1 (not $\overline{f}$). Also, for clarity we will now omit the coupling constants.

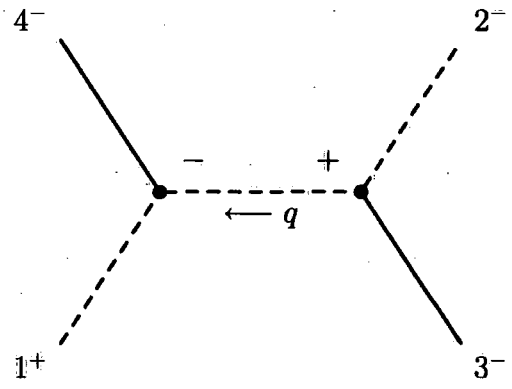

Figure 2.1: Diagram contributing to $A(\overline{f}_1^+, f_2^-, 3^-, 4^-)$. Fermion lines are dashed, photon lines are solid. All particles are incoming. There is also a similar diagram with photons 3 and 4 interchanged.

(2.17) we can evaluate the spinor products involving λ_q:

$$\begin{aligned} \langle \lambda_q\, 4\rangle &= \langle 4\, 1\rangle\, \phi_1\,, \\ \langle \lambda_q\, 1\rangle &= \langle 1\, 4\rangle\, \phi_4\,, \\ \langle 2\, \lambda_q\rangle &= \langle 2\, 3\rangle\, \phi_3\,, \\ q^2 &= (k_2+k_3)^2\,, \\ &= \langle 2\, 3\rangle [2\, 3]\,. \end{aligned} \tag{2.20}$$

Here $\phi_i = [\eta\ i]$ is a function of the (arbitrary) spinor η. Simplifying, we find

$$-2\frac{\langle 4\, 1\rangle}{[2\, 3]}\frac{\phi_1^2}{\phi_3\phi_4}\,. \tag{2.21}$$

To this we must add the contribution from the diagram with photons 3 and 4 interchanged, namely

$$-2\frac{\langle 3\ 1\rangle}{[2\ 4]}\frac{\phi_1^2}{\phi_4\phi_3}\ . \tag{2.22}$$

When we add these two terms we find that momentum conservation, which can be expressed as $\langle 1\ 4\rangle[4\ 2]+\langle 1\ 3\rangle[3\ 2]=0$, ensures that the sum vanishes, so that

$$A(\overline{f_1^+}, f_2^-, 3^-, 4^-) = 0 \tag{2.23}$$

as expected. In this simple case there was no need to fix the value of η, and we carried the dependence on it through to the end, through the ϕ_i functions. In more complicated calculations we will specify η as a spinor describing one of the external momenta, and thereby simplify our task.

The next demonstration of the MHV rules applied to QED processes that we will consider is the evaluation of the amplitude $A(\overline{f_1^+}, f_2^-, 3^-, 4^-, 5^+)$. We describe this as an $\overline{\text{MHV}}$ amplitude, as it has exactly the opposite helicity structure to an MHV amplitude, i.e. two positive helicities and the remainder negative. There are four diagrams (see Figure 2.2), though once again our task is simplified because there are only two independent expressions to work out, the rest being obtained by appropriate permutations. We find that

$$\begin{aligned} M &= 2\frac{\langle\lambda_q\ 4\rangle^2}{\langle\lambda_q\ 5\rangle\langle 1\ 5\rangle}\frac{1}{q^2}\sqrt{2}\frac{\langle 2\ 3\rangle^2}{\langle 2\ \lambda_q\rangle} \\ &= 2^{\frac{3}{2}}\frac{[\langle 4\ 1\rangle\phi_1+\langle 4\ 5\rangle\phi_5]^2}{[\langle 5\ 1\rangle\phi_1+\langle 5\ 4\rangle\phi_4]\langle 1\ 5\rangle[2\ 3]\phi_3} \end{aligned} \tag{2.24}$$

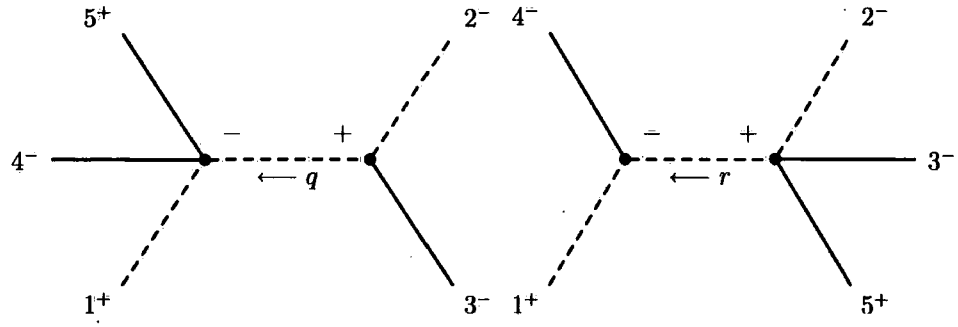

Figure 2.2: Diagrams contributing to $A(\overline{f_1^+}, f_2^-, 3^-, 4^-, 5^+)$. The $3 \leftrightarrow 4$ permutation of each also contributes.

and

$$\begin{aligned} N &= \sqrt{2}\frac{\langle \lambda_r\ 4\rangle^2}{\langle \lambda_r\ 1\rangle}\frac{1}{r^2}2\frac{\langle 2\ 3\rangle^2}{\langle \lambda_r\ 5\rangle\langle 2\ 5\rangle} \\ &= -2^{3/2}\frac{\langle 2\ 3\rangle^2\phi_1^2}{[\langle 5\ 2\rangle\phi_2 + \langle 5\ 3\rangle\phi_3]\langle 2\ 5\rangle[1\ 4]\phi_4}\,. \end{aligned} \tag{2.25}$$

If we choose $\eta = \widetilde{\lambda}_1$ then $\phi_1 = 0$ and so N and its $3 \leftrightarrow 4$ permutation vanish. We are left with two terms which, after again invoking momentum conservation, simplify to

$$A(\overline{f_1^+}, f_2^-, 3^-, 4^-, 5^+) = -2^{\frac{3}{2}}\frac{[1\ 2][1\ 5]^3[2\ 5]}{\prod_{k=3}^{5}[1\ k][2\ k]}\,. \tag{2.26}$$

Inspection of the corresponding MHV amplitude (2.10) shows that this result has the correct magnitude. Having made a particular choice of phase for the MHV amplitudes in (2.10), a definite phase emerges for their $\overline{\text{MHV}}$ counterparts. The former were chosen to be holomorphic functions of the

λ's of the external legs – they contain only $\langle..\rangle$ products. The latter emerge as anti-holomorphic, consisting only of $[..]$ products. Colour-ordered partial amplitudes also have this property. Here however, we are dealing with a physical amplitude, and so the phase is not a measurable quantity. It is interesting to note that choosing the MHV amplitudes to have different phases, for instance an expression containing a mixture of λ and $\tilde{\lambda}$, does *not* in general lead to correct results for non-MHV amplitudes. This is to be expected, as it is only those amplitudes which, apart from the momentum-conserving delta function, are comprised entirely of $\langle..\rangle$ products that transform simply onto a line in twistor space [16].

2.3.2 The NMHV amplitude $A(\overline{f_1^+}, f_2^-, 3^+, 4^+, 5^-, 6^-)$

Let us introduce the concept of a next-to-MHV amplitude and denote it NMHV. By this we mean one which has three negative helicity partons, with the remainder positive. The first non-zero NMHV amplitudes appear for $n = 4$ photons, when two photons have helicity $+$ and two have helicity $-$. There are eight diagrams for this process but only three distinct structures, so that we need only work out three diagrams and obtain the others by permuting photons. In fact, by a judicious choice of the arbitrary spinor η we can reduce the expression to just two independent terms plus permutations.

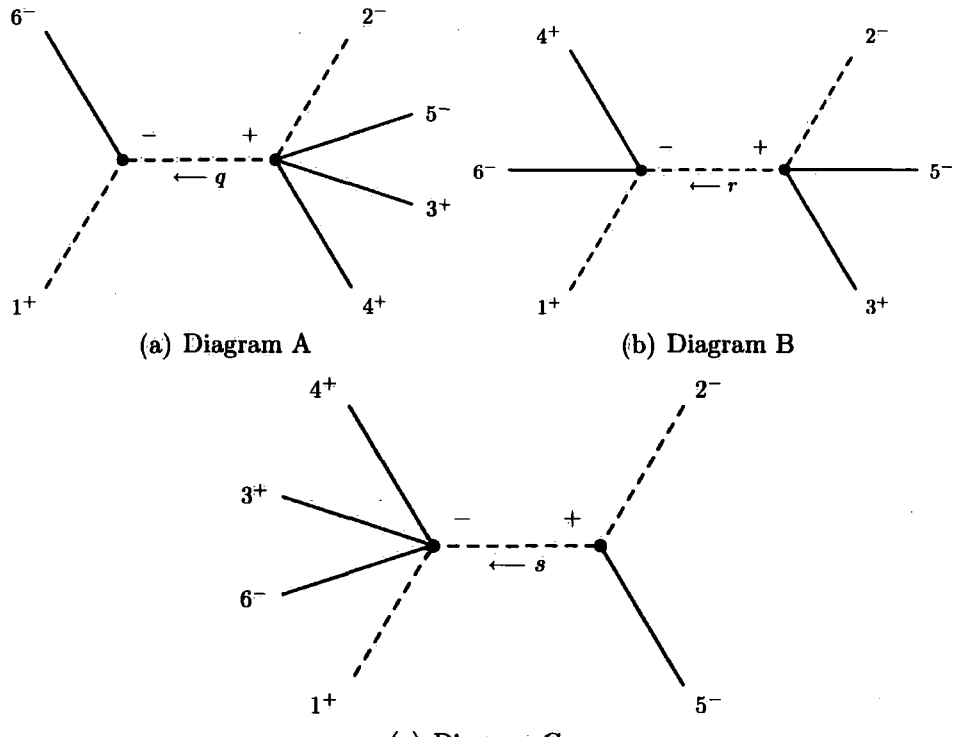

(a) Diagram A

(b) Diagram B

(c) Diagram C

Figure 2.3: Diagrams contributing to $A(\overline{f_1^+}, f_2^-, 3^+, 4^+, 5^-, 6^-)$. Various permutations of each also contribute.

Referring to Figure 2.3,

$$
\begin{aligned}
A &= -4\frac{\phi_1^2[\langle 2\ 1\rangle\phi_1 + \langle 2\ 6\rangle\phi_6]\langle 2\ 5\rangle^2}{[1\ 6]\phi_6\langle 2\ 3\rangle\langle 2\ 4\rangle[\langle 3\ 1\rangle\phi_1 + \langle 3\ 6\rangle\phi_6][\langle 4\ 1\rangle\phi_1 + \langle 4\ 6\rangle\phi_6]}\ , \\
B &= -4\frac{[\langle 6\ 1\rangle\phi_1 + \langle 6\ 4\rangle\phi_4]^2\langle 2\ 5\rangle^2}{[\langle 4\ 1\rangle\phi_1 + \langle 4\ 6\rangle\phi_6][\langle 3\ 2\rangle\phi_2 + \langle 3\ 5\rangle\phi_5]\langle 1\ 4\rangle r^2\langle 2\ 3\rangle}\ , \\
C &= -4\frac{[\langle 1\ 2\rangle\phi_2 + \langle 1\ 5\rangle\phi_5][\langle 6\ 2\rangle\phi_2 + \langle 6\ 5\rangle\phi_5]^2}{[\langle 3\ 2\rangle\phi_2 + \langle 3\ 5\rangle\phi_5][\langle 4\ 2\rangle\phi_2 + \langle 4\ 5\rangle\phi_5]\langle 1\ 3\rangle\langle 1\ 4\rangle[2\ 5]\phi_5}
\end{aligned}
\tag{2.27}
$$

If we choose $\eta = \widetilde{\lambda}_1$ then $\phi_1 = 0$ and the contribution from diagram A above vanishes. The other two terms simplify, and we end up with the following

expression,

$$\begin{aligned} A(\overline{f_1^+}, f_2^-, 3^+, 4^+, 5^-, 6^-) &= 4\frac{\langle 4\ 6\rangle[1\ 4]^2\langle 2\ 5\rangle^2}{\langle 1\ 4\rangle[1\ 6](p_2+p_3+p_5)^2\langle 2\ 3\rangle\langle 3|2+5|1]} \\ &+ (3 \leftrightarrow 4) + (5 \leftrightarrow 6) + \begin{pmatrix} 3 \leftrightarrow 4 \\ 5 \leftrightarrow 6 \end{pmatrix} \\ &+ 4\frac{(s_{12}+s_{15})\langle 6|2+5|1]^2}{\langle 1\ 3\rangle\langle 1\ 4\rangle[5\ 2][1\ 5]\langle 3|2+5|1]\langle 4|2+5|1]} \\ &+ (5 \leftrightarrow 6) \end{aligned} \tag{2.28}$$

Here we have introduced the shorthand notation

$$\langle i \mid j+k \mid l\,] = \langle i\ j\rangle[j\ l] + \langle i\ k\rangle[k\ l], \tag{2.29}$$

and $s_{ij} = 2\ p_i \cdot p_j$. The result above is obviously more complicated than the one-term MHV amplitudes, but it is still much simpler than what would be obtained via a Feynman diagram calculation. Although the two algebraic forms are very different, we have checked that this expression agrees numerically with the KS results [14], up to a phase. It is interesting to note that we do not have the freedom to introduce relative phases among the set of MHV amplitudes. For example, introducing a factor of -1 into the 1-photon MHV amplitude while leaving the others fixed will obviously lead to a change in the relative phases among the terms in (2.28). Our derived expression for $A(\overline{f_1^+}, f_2^-, 3^+, 4^+, 5^-, 6^-)$ will then no longer have the

correct magnitude. In this way an apparently unphysical phase affects physical cross sections. So the phases of the MHV amplitudes in (2.10) must be chosen appropriately. We have also calculated the NMHV 5-photon amplitude[5] $A(\overline{f}_1^+, f_2^-, 3^+, 4^+, 5^-, 6^-, 7^+)$ using the MHV rules, and once again found numerical agreement with [14]. We expect that further tests will be successful. Amplitudes with n photons, two of which have negative helicity, require the evaluation of only $n-1$ structures. The full set of diagrams is then easily obtained through permutations. Increasing the number of negative helicity photons leads to MHV diagrams with more than two vertices. For QED processes with two fermions, the absence of a pure-photon vertex means that such diagrams consist only of a linear string of vertices – there is no branching. Each vertex has one negative helicity photon attached to it, and the remaining photons are added in all possible ways.

2.3.3 Soft Limits

We have checked algebraically that (2.28) has the correct limits when one of the photon's momenta is taken to zero, namely that the expression tends to the amplitude in the absence of that photon, multiplied by a 'soft' factor

[5]Note that all non-zero $n = 5$ helicity amplitudes are either MHV or NMHV, as for $n = 4$. The first NNMHV amplitudes appear at $n = 6$.

called the eikonal factor:

$$A(\overline{f_1^+}, f_2^-, 3^+, 4^+, 5^-, 6^-) \xrightarrow{3\to 0} A(\overline{f_1^+}, f_2^-, 4^+, 5^-, 6^-) \times \frac{\sqrt{2}\langle 1\ 2\rangle}{\langle 1\ 3\rangle\langle 2\ 3\rangle}$$
$$A(\overline{f_1^+}, f_2^-, 3^+, 4^+, 5^-, 6^-) \xrightarrow{5\to 0} A(\overline{f_1^+}, f_2^-, 3^+, 4^+, 6^-) \times \frac{\sqrt{2}[1\ 2]}{[1\ 5][2\ 5]} \quad (2.30)$$

and similarly for the other photons. Notice that when a positive helicity photon becomes soft, the eikonal factor is comprised entirely of $\langle..\rangle$ spinor products, whereas when a negative helicity photon becomes soft the eikonal factor is comprised entirely of $[..]$ products. We have also verified that the amplitudes presented here have the correct collinear factorization properties when one of the photons is emitted in the direction of the incoming fermion or anti-fermion.[6]

2.4 The BCF Recursion Relations

A new set of recursion relations [28] has been proposed to calculate tree amplitudes in gauge theories. We will here give a brief review of this technique, before showing how the relations can be used, along with (2.10), to calculate QED amplitudes. Consider an n particle (purely gluonic, for definiteness) scattering amplitude, with arbitrary helicities. Choose two of the external lines to be 'hatted' – this will be defined shortly. Suppose the n-th (positive helicity) and $(n-1)$-th (negative helicity) gluons are hatted. These are

[6]The collinear behaviour of QCD MHV amplitudes has been studied in [26, 27].

reference lines. The BCF recursion relation then reads

$$A_n(1,2,\ldots,(n-1)^-,n^+) = \qquad (2.31)$$
$$\sum_{i=1}^{n-3}\sum_{h=+,-} A_{i+2}(\widehat{n},1,2,\ldots,i,-\widehat{P}^h_{n,i})\frac{1}{P^2_{n,i}}A_{n-i}(+\widehat{P}^{-h}_{n,i},i+1,\ldots,n-2,\widehat{n-1})$$

where

$$\begin{aligned}
P_{n,i} &= p_n + p_1 + \cdots + p_i \,, \\
\widehat{P}_{n,i} &= P_{n,i} + \frac{P^2_{n,i}}{\langle n-1|P_{n,i}|n]}\lambda_{n-1}\widetilde{\lambda}_n \,, \\
\widehat{p}_{n-1} &= p_{n-1} - \frac{P^2_{n,i}}{\langle n-1|P_{n,i}|n]}\lambda_{n-1}\widetilde{\lambda}_n \,, \\
\widehat{p}_n &= p_n + \frac{P^2_{n,i}}{\langle n-1|P_{n,i}|n]}\lambda_{n-1}\widetilde{\lambda}_n \,. \qquad (2.32)
\end{aligned}$$

Identities such as

$$\begin{aligned}
\langle \bullet\ \widehat{P}\rangle &= -\langle \bullet \mid P \mid n] \times \frac{1}{\omega} \,, \\
[\widehat{P}\ \bullet] &= -\langle n-1 \mid P \mid \bullet] \times \frac{1}{\bar{\omega}} \,, \qquad (2.33)
\end{aligned}$$

are used to remove the hats, whereupon the result can be simplified using standard spinor identities. Here $\omega = [\widehat{P}\ n]$ and $\bar{\omega} = \langle n-1\ \widehat{P}\rangle$. The factors ω and $\bar{\omega}$ only ever appear in the combination $\omega\bar{\omega} = \langle n-1\ |P\ |n]$. The procedure can be conveniently represented diagrammatically, see Figure 2.4

for a specific case.

In [17, 29] the relations were shown to work for amplitudes involving fermions, and in [30] it was shown that the reference gluons need not be either adjacent or of the same helicity. Applications to massive particles were described in [31–33]. The relations were proven in [30] by shifting the hatted momenta by a complex amount – see Section 2.5. Here we will be interested in applying the above recursion relation to QED processes. In contrast to the MHV rules, the recursion relations involve the use of $\overline{\text{MHV}}$ amplitudes. We can obtain these from (2.10) by switching $\langle..\rangle$ and $[..]$, and using charge conjugation invariance to swap the fermion and anti-fermion.

2.4.1 Example of BCF recursion relations applied to a QED process

Consider the MHV amplitude $A(\overline{f}_1^+, f_2^-, 3^+, 4^+, 5^-)$. As before, f and $\overline{f}$ denote a fermion and anti-fermion respectively, and i^+ represents a positive helicity photon of momentum k_i. Let us choose the hatted lines to be 1 and 5, as shown in Figure 2.4. Then there is only one distinct diagram[7] for this process, which evaluates to

$$\frac{\sqrt{2}[\widehat{1}\ 3]^2}{[\widehat{1}\ \widehat{P}]}\frac{1}{(k_1+k_3)^2}\frac{2\langle 2\ \widehat{5}\rangle^2}{\langle 2\ 4\rangle\langle \widehat{P}\ 4\rangle}\ . \tag{2.34}$$

[7]Note that as detailed in [28], diagrams with an upper vertex of $(+\,+\,-)$ or a lower vertex of $(-\,-\,+)$ vanish. We have not drawn such diagrams.

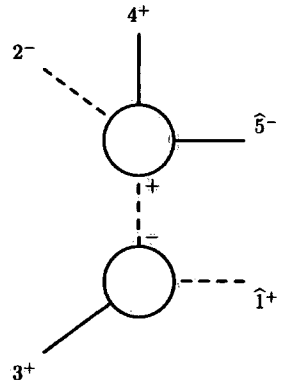

Figure 2.4: BCF Diagram contributing to $A(\overline{f}_1^+, f_2^-, 3^+, 4^+, 5^-)$. As usual, dashed lines are fermions, solid lines are photons.

Here we have used (2.10), together with its helicity flipped version, to substitute for the (on-shell) tree amplitudes in (2.31). $P = k_1 + k_3$ is the momenta of the internal line. Simplifying, we get

$$2\sqrt{2}\frac{\langle 2\ 5\rangle^2}{\langle 2\ 4\rangle\langle 3\ 4\rangle\langle 1\ 3\rangle}\ , \tag{2.35}$$

and to this we must add a similar expression with photons 3 and 4 interchanged,

$$2\sqrt{2}\frac{\langle 2\ 5\rangle^2}{\langle 2\ 3\rangle\langle 4\ 3\rangle\langle 1\ 4\rangle}\ . \tag{2.36}$$

After simplifying using Schouten's identity[8] we recover the expected result,

$$\begin{aligned} A(\overline{f}_1^+, f_2^-, 3^+, 4^+, 5^-) &= 2\sqrt{2}\frac{\langle 2\ 5\rangle^2}{\langle 2\ 4\rangle\langle 3\ 4\rangle\langle 1\ 3\rangle} + 2\sqrt{2}\frac{\langle 2\ 5\rangle^2}{\langle 2\ 3\rangle\langle 4\ 3\rangle\langle 1\ 4\rangle} \\ &= 2\sqrt{2}\frac{\langle 2\ 1\rangle\langle 2\ 5\rangle^3\langle 1\ 5\rangle}{\prod_{k=3}^{5}\langle 1\ k\rangle\langle 2\ k\rangle}\ . \end{aligned} \tag{2.37}$$

[8]For any 4 spinors $\langle a\ b\rangle\langle c\ d\rangle + \langle a\ c\rangle\langle d\ b\rangle + \langle a\ d\rangle\langle b\ c\rangle = 0$.

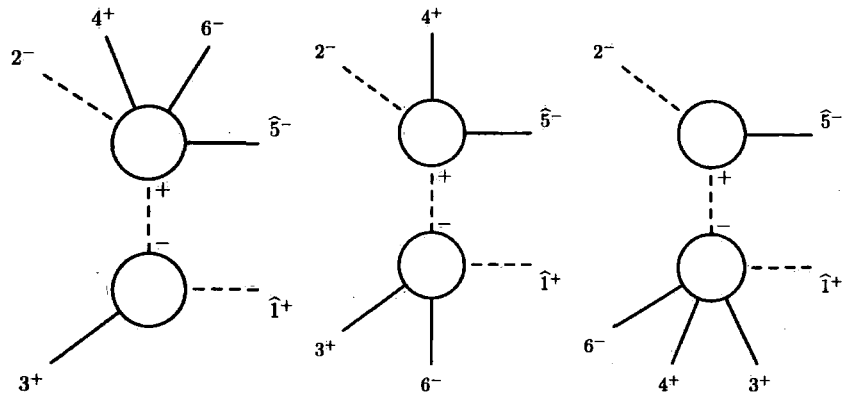

(a) Diagram P (b) Diagram Q (c) Diagram R

Figure 2.5: BCF diagrams contributing to $A(\overline{f_1^+}, f_2^-, 3^+, 4^+, 5^-, 6^-)$. Various permutations of each also contribute.

2.4.2 The NMHV amplitude $A(\overline{f_1^+}, f_2^-, 3^+, 4^+, 5^-, 6^-)$

There are three BCF diagrams for this process, up to permutations, which is the same one that we calculated in Section 2.3 using the MHV rules. We can build up the four photon process using amplitudes we have already calculated. The diagrams (Figure 2.5) evaluate to

$$\begin{aligned} P &= 4\frac{\langle 5|1+3|2]\langle 5|1+3|4]^2}{\langle 3|1+5|2]\langle 5|1+3|6](p_1+p_3+p_5)^2[2\ 6]\langle 1\ 3\rangle}\,, \\ Q &= 4\frac{\langle 2\ 5\rangle^2[3\ 1]^2\langle 5|3+6|1]}{\langle 2\ 4\rangle\langle 4|3+6|1]\langle 5|1+3|6](p_1+p_3+p_6)^2[6\ 1]}\,, \\ R &= 4\frac{\langle 6|2+5|1]^2(p_1+p_2+p_5)^2[2\ 1]^2}{\langle 3|2+5|1]\langle 4|2+5|1]\langle 3|1+5|2]\langle 4|1+5|2][5\ 1][2\ 5]}\,, \end{aligned} \tag{2.38}$$

where we have chosen external lines 1 and 5 to be hatted. The full result is then

$$A(\overline{f_1^+}, f_2^-, 3^+, 4^+, 5^-, 6^-) = (P+Q) + (3 \leftrightarrow 4) + R\,. \tag{2.39}$$

We have checked numerically that this expression is equal to (2.28) which was calculated using the MHV rules. Both are equal to the corresponding result obtained from the KS formula, up to a phase.

2.5 Proof Of the BCF Recursion Relations

An elegant proof of the recursion relations originally proposed in [28] was presented in [30]. Here we will briefly sketch its main elements, before discussing its applicability to QED.

Take a tree level amplitude $A(1,2,\ldots,n)$ with arbitrary helicities and

- choose two particles for special treatment, which we can take to be the k-th and l-th particles with helicities h_k and h_l respectively, and introduce a complex variable z to rewrite their momenta as

$$\begin{aligned} p_k(z) &= \lambda_k(\tilde{\lambda}_k - z\tilde{\lambda}_l) = p_k(0) - z\lambda_k\tilde{\lambda}_l \,, \\ p_l(z) &= (\lambda_l + z\lambda_k)\tilde{\lambda}_l = p_l(0) + z\lambda_k\tilde{\lambda}_l \,. \end{aligned} \tag{2.40}$$

We have effectively shifted the spinors $\lambda_l \to \lambda_l + z\lambda_k$ and $\tilde{\lambda}_k \to \tilde{\lambda}_k - z\tilde{\lambda}_l$. Note that there is no symmetry between k and l – they are treated differently. Having done this we can now construct the auxiliary function

$$A(z) = A(p_1, p_2, \ldots, p_k(z), \ldots, p_l(z), \ldots, p_n) \,. \tag{2.41}$$

The aim now is to use the analytic structure of this auxiliary function,

considered as a function of z, to gain information on the physically relevant object $A(0)$.

- $A(z)$ has only simple poles. This can be seen by noting that poles can only arise from propagators such as $1/K^2$, where K is the momenta of an internal line. If both p_l and p_k, or neither of them, are present in the sum of external momenta contributing to K then the latter is independent of z and there is no z-pole in the propagator. However, if only one and not the other is present then the momenta of the internal line is linearly dependent on z. Thus $A(z)$ has only simple poles.

- Cauchy's theorem tells us that

$$A(0) = -\sum_{\alpha} \text{Residue}\left(\frac{A(z)}{z}\right)_{z=z_\alpha} - \text{Residue}\left(\frac{A(z)}{z}\right)_{z=\infty} \tag{2.42}$$

so that the physical amplitude $A(0)$ is fully determined by the finite pole positions z_α and residues of the auxiliary function, provided $A(z)$ vanishes at infinity. The finite residues are just products of lower-n tree amplitudes, with Feynman propagators in between. The recursion relation then follows immediately.

To demonstrate the vanishing of $A(z)$ as $z \to \infty$, one may use the MHV rules outlined in [22]. It suffices to show that the MHV amplitudes themselves vanish in this limit since, as shown in [30], the off-shell continuation does not affect the large z behaviour of a general MHV diagram. It turns out that

some choices of reference lines are allowed (i.e. lead to an auxiliary function that vanishes at infinity), whilst others are not. We can formulate some rules to determine the allowed choices. This is useful because, as the authors of Ref. [17] found, the number of BCF diagrams contributing to a given amplitude depends strongly on the reference lines chosen. A careful choice can save much labour, and yield more compact expressions.

First, let us repeat (2.10) for convenience,

$$A(\overline{f}^+, f^-, 1^+, 2^+ ..., I^-, ..., n^+) = \frac{2^{\frac{n}{2}} \langle f\overline{f}\rangle^{n-2} \langle fI\rangle^3 \langle \overline{f}I\rangle}{\prod_{i=1}^n \langle fi\rangle \langle \overline{f}i\rangle}, \tag{2.43}$$

and also its $\overline{\text{MHV}}$ counterpart

$$A(\overline{f}^+, f^-, 1^-, 2^-, ..., I^+, ..., n^-) \doteq \frac{2^{\frac{n}{2}} [\overline{f}f]^{n-2} [\overline{f}I]^3 [fI]}{\prod_{i=1}^n [fi][\overline{f}i]}. \tag{2.44}$$

The MHV rules can be employed using either solely MHV or solely $\overline{\text{MHV}}$ amplitudes. If we choose l to be a positive helicity photon, and consider (2.43) then it is clear that the amplitude vanishes at infinity since there are more factors of z in the denominator than in the numerator. This is true regardless[9] of the identity of k. Similarly if we choose k to be a negative helicity photon, and consider (2.44) then once again $A(z)$ vanishes at infinity, regardless of our choice of l. So in both these cases, which cover a large subset of the possible choices, the recursion relations will work. The positive helicity

[9] In fact if k is either the fermion or antifermion, then $A(z)$ vanishes as $1/z$ whereas if k is another photon then $A(z)$ vanishes as $1/z^2$.

anti-fermion may be used at the lower vertex provided the fermion is not used at the upper vertex, as in this case the MHV amplitude does not vanish as $z \to \infty$.

It is also possible [30] to see the analytic structure of an amplitude by considering the set of Feynman diagrams that contribute to it. For $e^+e^- \to n\gamma$ there are $n!$ diagrams, differing only in the order in which the photons are attached to the fermion line. The z-dependence of the diagram can only come from propagators (which either contribute a factor $1/z$ or are independent of z) and photon polarization vectors[10] which, in the spinor helicity formalism, take the general form

$$\epsilon^-_{a\dot{a}} = \frac{\lambda_a \tilde{\mu}_{\dot{a}}}{[\tilde{\lambda}\ \tilde{\mu}]}, \quad \epsilon^+_{a\dot{a}} = \frac{\mu_a \tilde{\lambda}_{\dot{a}}}{\langle \mu\ \lambda \rangle} \tag{2.45}$$

for negative and positive helicity photons respectively. Here μ and $\tilde{\mu}$ are reference spinors. Recall that we shift the spinors representing the momenta of the l-th and k-th legs as

$$\begin{aligned} \lambda_l &\to \lambda_l + z\lambda_k \\ \tilde{\lambda}_k &\to \tilde{\lambda}_k - z\tilde{\lambda}_l \end{aligned} \tag{2.46}$$

so that the polarization vector of the k-th photon behaves as $1/z$ if it has negative helicity and linearly in z if it has positive helicity. The opposite

[10] In contrast to QCD, the vertices are momentum independent and so cannot depend on z.

holds for the l-th photon. By inspecting the set of Feynman graphs we can deduce that choosing $h_k = -$ or $h_l = +$ is always allowed (leads to an $A(z)$ which vanishes at $z \to \infty$). This agrees with what we concluded above based on a consideration of the MHV diagrams.

2.6 Conclusions

We have shown that the modern techniques inspired by the transformation of Yang-Mills scattering amplitudes to twistor space [16] can be successfully applied to QED processes, and yield reasonably compact expressions. As well as some simple $\overline{\text{MHV}}$ amplitudes, we calculated the NMHV amplitude $A(\overline{f_1^+}, f_2^-, 3^+, 4^+, 5^-, 6^-)$ using both the MHV rules and BCF recursion approaches. The expressions obtained are not obviously equal, but numerical checks proved them to be so and the results were confirmed by comparison with the KS [14] formula, which is directly derived from Feynman diagrams. We have also checked that the amplitudes have the correct factorising (eikonal) form when one of the photons becomes soft. Note that the QED NMHV amplitudes we have presented can also in principle be obtained by symmetrizing QCD colour-ordered amplitudes, but this is a laborious procedure and will not lead directly to compact expressions. We have shown that it is possible, and much easier, to use *physical* MHV amplitudes directly in the MHV rules.

We have given explicit expressions for up to and including 4-photon am-

plitudes. The extension to $n \geq 5$ photons is in principle straightforward – in either the CSW or BCF approaches – although there is an inevitable growth in complexity as more $\mathrm{N}^n\mathrm{MHV}$ amplitudes start to appear. We have not been able to discern any large-n simplification of the expressions, in contrast to the remarkably compact expression for arbitrary n (see Eq. (2.6)) in the KS approach.

Chapter 3

Amplitudes with Massive Fermions

3.1 Introduction

In the previous chapter we described two new methods for evaluating multi-particle scattering amplitudes in gauge field theories. Both of these grew out of Witten's observation [16] that the simplicity of the so-called MHV amplitudes is mirrored by an interesting structure when the same amplitudes are expressed in terms of twistor space variables. These two methods are generally known as the 'MHV Rules' [22] and the BCF recursion relations [28]. In their initial forms, both schemes were restricted to amplitudes involving only massless partons. However, it is important phenomenologically to be able to deal with massive fermions. We will see in the final chapter that the

amplitude with a pair of massive quarks and three gluons will be relevant to studies of Central Exclusive Production at the LHC.

It was shown in Ref. [34] how to generalise Supersymmetric Ward Identities [35, 36] to include massive particles. In this way, different amplitudes involving fields belonging to the same supersymmetric multiplet are related by a rotation. For instance [37], amplitudes involving quarks and gluons are related by SWIs to amplitudes involving scalars and gluons, and these have been calculated in Ref. [33]. The off-shell Berends-Giele [21] recursion has also proved useful [38]. Tree amplitudes with massive fermions are required as input within the unitarity [39, 40] method to calculate one-loop amplitudes, and to this end Ref. [41] provides four- and five-point amplitudes with D-dimensional fermions, calculated using BCF recursion.

The BCF recursion relations were extended in Ref. [31] to include massive fermions, and in [32] four-point amplitudes involving two massive quarks and two gluons were calculated. Five point amplitudes with massive fermions have so far not been treated using BCF recursion. The goal of the present work is to explore the utility of BCF recursion to four and five point amplitudes with massive fermions. We find that a treatment of massive fermion spinors introduced some twenty years ago in Ref. [14] proves to be very useful. This treatment of massive spinor products was outlined in the introduction. In this chapter we will demonstrate the use of BCF recursion in calculating some simple scattering processes with massive quarks in QCD. We will use $2 \to 2$ amplitudes as building blocks for the evaluation of the

phenomenologically relevant $gg \to b\bar{b}g$ colour-ordered partial amplitudes. As will be explained in Chapter 5, these are relevant for the calculation of colour-singlet cross sections, which are backgrounds to central exclusive production of Higgs bosons.

3.2 Four Point Amplitudes: $\bar{q}q \to gg$

To demonstrate the use of the massive spinor products described in the previous section we calculate the helicity amplitudes $M^{\lambda_1\lambda_2\lambda_3\lambda_4}$ for the simple QCD process $\bar{q}^{\lambda_1}(p_1)\, q^{\lambda_2}(p_2) \to g^{\lambda_3}(p_3)\, g^{\lambda_4}(p_4)$. The $\lambda_1, \lambda_2 = \pm$ labels on the quarks refer to their spin polarisations in the sense already indicated. If we choose k_0 appropriately then they can be thought of as helicity labels. We will evaluate the partial (colour) amplitudes for the above scattering process, i.e. we consider contributions only from those diagrams with a particular ordering of the external gluons. The full colour-summed amplitudes can then be recovered by inserting appropriate colour factors, as described in Chapter 1.

We first consider the M^{+-+-} partial amplitude, for which there are two Feynman diagrams, shown in Figure 3.1. We will express them in terms of massive spinor products. For the slashed gluon polarisation vectors we use

$$\not{\epsilon}^{+}(p,k) = \sqrt{2}\,\frac{u_+(k)\bar{u}_+(p) + u_-(p)\bar{u}_-(k)}{\langle kp\rangle}, \tag{3.1}$$

$$\not{\epsilon}^{-}(p,k) = \sqrt{2}\,\frac{u_+(p)\bar{u}_+(k) + u_-(k)\bar{u}_-(p)}{[pk]}, \tag{3.2}$$

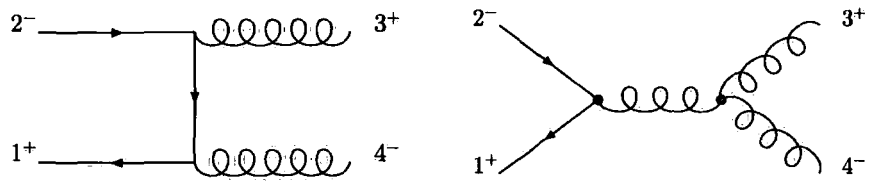

(a) Diagram A (b) Diagram B

Figure 3.1: Diagrams contributing to the colour-ordered partial amplitude for the process $\bar{q}^+(p_1)q^-(p_2) \to g^+(p_3)g^-(p_4)$.

where k is a (null) reference vector which may be chosen separately for each gluon. Different choices of reference vector amount to working in different gauges. The choice $k_3 = p_4$ and $k_4 = p_3$ is particularly convenient in this context, as Diagram B vanishes in this gauge. We have for the other diagram

$$\bar{u}^+(p_1)\,\frac{\not{\epsilon}^-(p_4)}{\sqrt{2}}\,\frac{\not{p}_2 - \not{p}_3 + m}{(p_2-p_3)^2 - m^2}\,\frac{\not{\epsilon}^+(p_3)}{\sqrt{2}}\,u^-(p_2), \tag{3.3}$$

which simplifies easily to

$$\bar{u}^+(p_3)\not{p}_2 u^+(p_4)\,\frac{\bar{u}^+(p_1)\big[u^-(p_3)\bar{u}^-(p_4) + u^+(p_4)\bar{u}^+(p_3)\big]u^-(p_2)}{4\,p_3\cdot p_4\;p_4\cdot p_1}, \tag{3.4}$$

so that

$$M^{+-+-} = [3|2|4\rangle\frac{[13](42) + (14)[32]}{4\,p_3\cdot p_4\;p_4\cdot p_1}. \tag{3.5}$$

As promised, we are left with an expression for the amplitude in terms of vector products and massive spinor products. We next consider the other $M^{\lambda_1\lambda_2+-}$ amplitudes. It is interesting to note that these are directly obtained from the M^{+-+-} amplitude simply by changing the type of certain brackets.

Thus

$$M^{+++-} = [3|2|4\rangle \frac{[13]\langle 42\rangle + \langle 14\rangle[32]}{4\, p_3 \cdot p_4\; p_4 \cdot p_1}, \tag{3.6}$$

$$M^{--+-} = [3|2|4\rangle \frac{\langle 13\rangle\langle 42\rangle + \langle 14\rangle[32]}{4\, p_3 \cdot p_4\; p_4 \cdot p_1}, \tag{3.7}$$

$$M^{-++-} = [3|2|4\rangle \frac{\langle 13\rangle\langle 42\rangle + \langle 14\rangle\langle 32\rangle}{4\, p_3 \cdot p_4\; p_4 \cdot p_1}. \tag{3.8}$$

Those amplitudes where the gluons have helicities $(-\ +)$ can be obtained directly from the ones above by complex conjugation. Let us now examine the case where the gluons have the same helicity. By direct calculation we find

$$M^{--++} = m[43] \frac{\langle 13\rangle\langle 42\rangle - \langle 14\rangle\langle 32\rangle}{\langle 34\rangle^2\; 2\; p_4 \cdot p_1}, \tag{3.9}$$

from which we deduce

$$M^{++++} = m[43] \frac{\langle 13\rangle\langle 42\rangle - \langle 14\rangle\langle 32\rangle}{\langle 34\rangle^2\; 2\; p_4 \cdot p_1}, \tag{3.10}$$

$$M^{+-++} = 0, \tag{3.11}$$

$$M^{-+++} = m[43] \frac{\langle 13\rangle\langle 42\rangle - \langle 14\rangle\langle 32\rangle}{\langle 34\rangle^2\; 2\; p_4 \cdot p_1}, \tag{3.12}$$

$$= \frac{m[34]\langle 12\rangle}{\langle 34\rangle\; 2\; p_4 \cdot p_1}, \tag{3.13}$$

where in the last line we have used the Schouten identity. The amplitudes with two negative helicity gluons are obtained via complex conjugation. There are several interesting things to note about these results. First, the

amplitude M^{+-++} vanishes (for any choice of k_0) because of the identity[1] $(13)(42) - (14)(32) = 0$. Second, when k_0 is parallel to the line of approach of the fermions (i.e. when we work in the helicity basis) then the product $\langle 12\rangle$, and hence M^{-+++}, vanishes.

We have verified that when squared and summed over spins and colours, the set of $2 \to 2$ scattering amplitudes given above matches the well-known result (see for example Ref. [42]) calculated using Feynman diagrams and 'trace technology', namely

$$\sum_{\text{colours}} \sum_{\text{spins}} |M|^2 = 256 \left(\frac{1}{6\tau_1\tau_2} - \frac{3}{8}\right)\left(\tau_1^2 + \tau_2^2 + \rho - \frac{\rho^2}{4\tau_1\tau_2}\right), \qquad (3.14)$$

where

$$\tau_1 = \frac{2p_1 \cdot p_3}{s}, \quad \tau_2 = \frac{2p_1 \cdot p_4}{s}, \quad \rho = \frac{4m^2}{s}, \quad s = (p_1 + p_2)^2. \qquad (3.15)$$

Finally, the $m \to 0$ behaviour of the spin amplitudes can easily be read off from the expressions given above. For example, if E denotes the typical scale

[1] See Chapter 1 for a list of identities and notation.

of the $2 \to 2$ scattering[2], then in the $m/E \to 0$ limit we have

$$\begin{aligned} M^{++\pm\mp},\ M^{--\pm\mp} &\sim O(1), \\ M^{+-\pm\mp},\ M^{-+\mp\pm} &\sim O(m/E), \\ M^{++\pm\pm},\ M^{--\mp\mp} &\sim O(m^2/E^2), \\ M^{+---},\ M^{-+++} &\sim O(m/E), \\ M^{+-++},\ M^{-+--} &= 0. \end{aligned} \tag{3.16}$$

Note that in deriving these results we have assumed that k_0 is *not* directed along any of the particle momenta, so that all $\langle ij \rangle$ spinor products are $O(m)$ in the $m \to 0$ limit, and $\langle ij \rangle$, $[ij]$ products are $O(E)$. If on the other hand we choose the (fermion) helicity basis by taking k_0 in the direction of (say) p_1, then (3.16) becomes

$$\begin{aligned} M^{+-\pm\mp},\ M^{-+\mp\pm} &\sim O(1), \\ M^{+-\pm\pm},\ M^{-+\mp\mp} &= 0, \\ M^{++\pm\mp},\ M^{--\mp\pm} &\sim O(m/E), \\ M^{++++},\ M^{----} &\sim O(m/E), \\ M^{--++},\ M^{++--} &\sim O(m^3/E^3). \end{aligned} \tag{3.17}$$

[2]We explicitly exclude zero angle scattering.

3.3 BCFW Recursion

In this section we will use the BCF recursion relations [28] to evaluate five parton QCD amplitudes with a pair of massive fermions. The recursion involves *on-shell* amplitudes with momenta shifted by a complex amount. We will use the $2 \to 2$ results of the previous section as building blocks for this calculation. A description of the recursion, and an outline of its proof, was given in Chapter 2. We will here present the recursion in a form more appropriate for discussing the inclusion of massive partons.

We begin by choosing two massless[3] particles i and j whose slashed momenta we shift as follows,

$$\begin{aligned} \not{p}_i \to \hat{\not{p}}_i &= \not{p}_i + z\not{\eta}, \\ \not{p}_j \to \hat{\not{p}}_j &= \not{p}_j - z\not{\eta}, \end{aligned} \tag{3.18}$$

where

$$\not{\eta} = u^+(p_j)\bar{u}^+(p_i) + u^-(p_i)\bar{u}^-(p_j) \tag{3.19}$$

is such that both p_i and p_j remain on-shell. Using the familiar spin-sum condition, which is valid for massless p,

$$\sum_\lambda u^\lambda(p)\ \bar{u}^\lambda(p) = \not{p} \tag{3.20}$$

[3]It should be noted that by only hatting massless external legs we are restricting ourselves to amplitudes with at least two massless particles.

we can re-express the shift (3.18) as a shift of spinors:

$$u^+(p_i) \rightarrow u^+(\widehat{p}_i) = u^+(p_i) + z\, u^+(p_j), \tag{3.21}$$

$$\bar{u}^-(p_i) \rightarrow \bar{u}^-(\widehat{p}_i) = \bar{u}^-(p_i) + z\, \bar{u}^-(p_j), \tag{3.22}$$

$$\bar{u}^+(p_j) \rightarrow \bar{u}^+(\widehat{p}_j) = \bar{u}^+(p_j) - z\, u^+(p_i), \tag{3.23}$$

$$u^-(p_j) \rightarrow u^-(\widehat{p}_j) = u^-(p_j) - z\, u^-(p_i). \tag{3.24}$$

In the Weyl spinor notation we are shifting λ_i and $\widetilde{\lambda}_j$. For massless particles, Dirac 4-spinors are effectively two copies of a Weyl 2-spinor, hence the four shifts of (3.21)–(3.24). Notice that there is no symmetry between i and j — they are treated differently.

The amplitude is now a complex function of the parameter z. What the authors of [30] showed was that we can use the analytic properties of the amplitude as a function of z to glean information about the physical case $z = 0$. In particular, we get a recursion relation, which can be stated as

$$A_n = \sum_{\text{partitions}} \sum_{s} A_L(\widehat{p}_i, \widehat{P}^{-s})\, \frac{1}{P^2 - m_P^2}\, A_R(-\widehat{P}^s, \widehat{p}_j). \tag{3.25}$$

where the hatted quantities are the shifted momenta. In fact, this is only valid if the helicities of the marked particles are chosen appropriately. The marked particles are the i and j external lines, as described above. The recursion relations were also described in the previous chapter, and Eq. (3.25) is equivalent to Eq. (2.31). The crucial property which must be retained

if (3.25) is to hold is that the shifted amplitude must vanish in the limit $z \to \infty$. There are rules [17, 30–32] detailing which marking prescriptions are permitted in different cases. For our purposes, we will be on safe ground if the shifted gluons have helicites $(h^i, h^j) = (+, -)$ or $(\pm, \pm)$.

This method of calculation is particularly efficient because much of the computational complexity encountered in a Feynman diagram calculation is avoided since the lower point amplitudes A_L and A_R can be maximally simplified *before* being inserted in (3.25).

The sum is over all partitions of the particles into a 'left' group and a 'right' group, subject to the requirement that particles i and j are on opposite sides of the divide. The sum over s is a sum over the spins of the internal particle. Each diagram is associated with a particular value for the complex parameter z, which can be found via the condition that the internal momentum $\widehat{P}$ is on-shell. Note that $\widehat{P}$ is always a function of z because of the restriction that the marked particles i and j appear on opposite sides of the divide.

One useful point to note in practice is that three-point gluon vertices vanish for certain marking choices. In particular, for the j side of the diagram a gluon vertex with helicites $(+\,+\,-)$ vanishes, as does the combination $(-\,-\,+)$ on the i side. This was pointed out in Ref. [28].

We will be concerned in this work with the process $gg \to b\bar{b}g$, and so will encounter recursive diagrams connected by an internal fermion, the propagator of which is, in this formalism, the same as that of a scalar. Following

Ref. [32], we 'strip' fermions from the lower point amplitudes which feed the recursion and write

$$A_n = \sum_{\text{partitions}} \sum_{s} A_L(\widehat{p}_i, \widehat{P}^*) \frac{u_s(\widehat{P})\bar{u}_s(\widehat{P})}{P^2 - m_P^2} A_R(-\widehat{P}^*, \widehat{p}_j), \quad (3.26)$$

$$= \sum_{\text{partitions}} A_L(\widehat{p}_i, \widehat{P}^*) \frac{\widehat{\not{P}} + m_P}{P^2 - m_P^2} A_R(-\widehat{P}^*, \widehat{p}_j). \quad (3.27)$$

where P^* shows that the amplitude has been stripped of this external spinor wave-function. By way of example, let us reconsider the process $\bar{q}_1^+ q_2^- \to g_3^+ g_4^-$. We mark the gluons such that $i = 3$ and $j = 4$. Then there is one recursive diagram,

$$\bar{u}^+(p_1) \frac{\not{\epsilon}^-(\widehat{p}_4)}{\sqrt{2}} \frac{\not{p}_2 - \not{\widehat{p}}_3 + m}{(p_2 - p_3)^2 - m^2} \frac{\not{\epsilon}^+(\widehat{p}_3)}{\sqrt{2}} u^-(p_2). \quad (3.28)$$

With the shifts we have chosen, the hats on the polarisation vectors can be removed. The shifted part of the internal propagator is killed by either of the polarisation vectors. So in fact all the hats can be removed in (3.28), which is then identical to the Feynman diagram expression (3.3).

3.4 $\bar{q}q \to 3g$ from BCFW Recursion

The four-point amplitudes we derived in Section 3.2 are in such a form that it is trivial to strip a fermion off in the manner described above. This means that they are particularly convenient for use in BCFW recursion. Consider

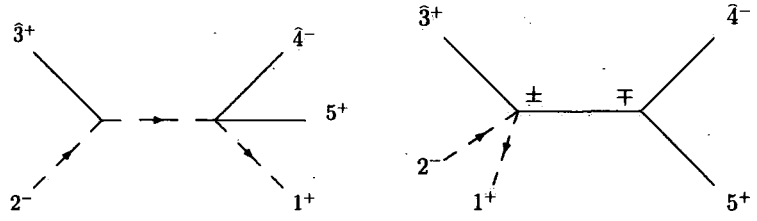

(a) Diagram A (b) Diagram B

Figure 3.2: Recursive diagrams contributing to $\bar{q}^+(p_1)q^-(p_2) \to g^+(p_3)g^-(p_4)g^+(p_5)$.

the process $\bar{q}_1^+ q_2^- \to g_3^+ g_4^- g_5^+$, for which there are three recursive diagrams, shown in Fig. 3.2. We choose the marking prescription $i = 3$, $j = 4$.

The two diagrams with internal gluons both vanish, due to the vanishing of M^{+--++} and the vanishing of the $(++-)$ gluon vertex with the shifts we have chosen. For the remaining diagram we use

$$M^{+--+} = -[4\|1\|3\rangle \frac{(13)[42] + [14](32)}{4\, p_3 \cdot p_4\; p_4 \cdot p_1}, \tag{3.29}$$

and strip the fermion $u^-(p_2)$, leaving

$$M^{+\bullet-+} = -[4\|1\|3\rangle\; \bar{u}^+(p_1)\; \frac{u^+(p_3)\bar{u}^+(p_4) + u^-(p_4)\bar{u}^-(p_3)}{4\, p_3 \cdot p_4\; p_4 \cdot p_1}. \tag{3.30}$$

After the appropriate relabelling this can be used in Diagram A, which can

then be written

$$A = -[5|1|\widehat{4}\rangle\ \bar{u}^+(p_1)\ \frac{u^+(\widehat{p}_4)\bar{u}^+(p_5) + u^-(p_5)\bar{u}^-(\widehat{p}_4)}{4\ p_5\cdot\widehat{p}_4\ p_5\cdot p_1}\ \frac{(\not{p}_2 - \not{\widehat{p}}_3 + m)}{(p_2-p_3)^2-m^2}$$
$$\times\ \frac{\not{\epsilon}^+(\widehat{p}_3)}{\sqrt{2}}u^-(p_2). \tag{3.31}$$

Due to our choice of marking, all the hats in the numerator can be removed. The shifted part of the propagator is killed by the gluon polarisation vector. We are left with

$$M^{+-+-+} = [5|1|4\rangle\left[\frac{m\langle 14\rangle\langle 42\rangle[53] + [15](42)[3|2|4\rangle - \langle 14\rangle[32][5|1|4\rangle}{8\ p_5\cdot p_1\ p_2\cdot p_3\ \widehat{p}_4\cdot p_5\ \langle 43\rangle}\right]. \tag{3.32}$$

We can work out z from the requirement that $\widehat{P}^2 = (p_2 - \widehat{p}_3)^2 = m^2$, and find

$$z = \frac{-2\ p_2\cdot p_3}{[3|2|4\rangle}. \tag{3.33}$$

The product $\widehat{p}_4\cdot p_5$ is then

$$\widehat{p}_4\cdot p_5 = (p_4 - z\ \eta)\cdot p_5 \tag{3.34}$$
$$= p_4\cdot p_5 + \frac{p_2\cdot p_3}{[3|2|4\rangle}[3|5|4\rangle. \tag{3.35}$$

The result (3.32) is much more compact than the expression obtained from a Feynman diagram calculation, with which it agrees. See Section 5 for the Feynman results for this process in terms of massive spinor products. We have checked that the expression (3.32) behaves as expected in the soft gluon

limit. That is, as a particular gluon becomes soft, the amplitude factorizes into a $2 \to 2$ amplitude multiplied by a universal 'eikonal factor'.

3.4.1 Results for Helicity Conserving Amplitudes

Here we give all the helicity conserving QCD amplitudes for $\bar{q}q \to ggg$. By helicity conserving we mean those amplitudes where the spin polarisations of the fermions are $+-$, in the sense described in the introduction. Whether these labels actually correspond physically to helicity depends on the choice of k_0. We choose to mark adjacent gluons, so that each amplitude has contributing recursive diagrams of the form of Fig. 3.2, that is, we have a diagram with an internal fermion and a diagram with an internal gluon. The vanishing of the $2 \to 2$ amplitude M^{+-++} simplifies those cases where there is a majority of positive helicity gluons. In particular, the diagrams with an internal gluon vanish. In the remaining cases, we evaluate such diagrams in the same way as in Ref. [28], using identities such as

$$[A\widehat{P}] = \frac{[A|P|i\rangle}{\langle \widehat{P} i\rangle}, \tag{3.36}$$

$$\langle \widehat{P} B\rangle = \frac{[j|P|B\rangle}{[j\widehat{P}]}, \tag{3.37}$$

with i and j as in (3.18). These identities hold only when A, B and the marked particles i and j are massless.

The results presented here are valid for arbitrary spin polarisations. Choosing a polarisation basis amounts to choosing the vector k_0, and when this is

done the expressions below will simplify. In the helicity basis for example, in which we choose k_0 to be parallel to the line of approach of the fermions, the building block M^{+---} vanishes. This causes the first term in each of the mostly-minus amplitudes below to vanish.

$$M^{+-+-+} = [5|1|4\rangle \left[\frac{m(14)(42)[53] + [15](42)[3|2|4\rangle - (14)[32][5|1|4\rangle}{8\, p_5\cdot p_1\; p_2\cdot p_3\; \widehat{p}_4\cdot p_5\; \langle 43\rangle}\right] \tag{3.38}$$

where $i = 3$, $j = 4$ and

$$\widehat{p}_4\cdot p_5 = p_4\cdot p_5 + \frac{p_2\cdot p_3}{[3|2|4\rangle}[3|5|4\rangle.$$

$$M^{+-++-} = [\widehat{4}|1|5\rangle\times$$
$$\left[\frac{m[1\widehat{4}][32]\langle 54\rangle + [1\widehat{4}](42)[3|2|5\rangle + 2p_5\cdot p_1(15)[32] + m(15)(42)[43]}{8\, p_2\cdot p_3\; \widehat{p}_4\cdot p_5\; p_5\cdot p_1\langle 43\rangle}\right] \tag{3.39}$$

where $i = 3$, $j = 4$ and

$$\widehat{p}_4\cdot p_5 = p_4\cdot p_5 + \frac{p_2\cdot p_3}{[3|2|4\rangle}[3|5|4\rangle, \qquad |\widehat{4}] = |4] - \frac{(-2\; p_2\cdot p_3)}{[3|2|4\rangle}|3].$$

$$M^{+--++} = [\widehat{4}|2|3\rangle \times$$
$$\left[\frac{m[\widehat{42}][15]\langle 43\rangle - [\widehat{42}](14)[5|1|3\rangle - 2p_2\cdot p_3[15](32) + m(14)(32)[54]}{8\ p_2\cdot p_3\ p_3\cdot\widehat{p}_4\ p_5\cdot p_1\langle 54\rangle}\right] \tag{3.40}$$

where $i = 5$, $j = 4$ and

$$p_3\cdot\widehat{p}_4 = p_3\cdot p_4 + \frac{p_1\cdot p_5}{[5|1|4\rangle}[5|3|4\rangle, \qquad |\widehat{4}] = |4] - \frac{(-2\ p_1\cdot p_5)}{[5|1|4\rangle}|5].$$

$$M^{+-+--} = \frac{m[21]\langle 45\rangle^3}{\langle 34\rangle\left[\langle 35\rangle 2p_5\cdot p_1 + \langle 34\rangle[4|2|5\rangle\right](p_1+p_2)^2} +$$
$$[3|2|\widehat{4}\rangle\left[\frac{m(\widehat{42})(15)[43] - (\widehat{42})[14][3|1|5\rangle - 2p_2\cdot p_3(15)[32] + m[14][32]\langle 54\rangle}{8\ p_2\cdot p_3\ p_3\cdot\widehat{p}_4\ p_5\cdot p_1[54]}\right] \tag{3.41}$$

where $i = 4$, $j = 5$, and

$$p_3\cdot\widehat{p}_4 = p_3\cdot p_4 + \frac{p_1\cdot p_5}{[4|1|5\rangle}[4|3|5\rangle, \qquad (\widehat{42}) = (42) + \frac{(2p_1\cdot p_5)}{[4|1|5\rangle}(52).$$

$$M^{+--+-} = \frac{m[21]\langle 53\rangle^4}{\sqrt{2}\,\langle 43\rangle\langle 45\rangle\left[\langle 53\rangle 2\,p_2\cdot p_3 + \langle 54\rangle[4|2|3\rangle\right](p_1+p_2)^2} \qquad (3.42)$$
$$+ \;[4|1|5\rangle\left[\frac{m[14][42]\langle 53\rangle + (15)[42][4|2|3\rangle - [14](32)[4|1|5\rangle}{8\,p_5\cdot p_1\;p_2\cdot p_3\;\widehat{p}_4\cdot p_5[34]}\right]$$

where $i = 4$, $j = 3$, and

$$\widehat{p}_4\cdot p_5 = p_4\cdot p_5 + \frac{p_2\cdot p_3}{[4|2|3\rangle}[4|5|3\rangle.$$

$$M^{+---+} = \frac{m[21]\langle 43\rangle^3}{\sqrt{2}\,\langle 45\rangle\left[\langle 53\rangle 2\,p_2\cdot p_3 + \langle 54\rangle[4|2|3\rangle\right](p_1+p_2)^2} + \qquad (3.43)$$
$$[5|1|\widehat{4}\rangle\times\left[\frac{m(1\widehat{4})(32)[54] + (1\widehat{4})[42][5|2|3\rangle + 2p_5\cdot p_1[15](32) + m[15][42]\langle 43\rangle}{8\,p_2\cdot p_3\;\widehat{p}_4\cdot p_5\;p_5\cdot p_1[34]}\right]$$

where $i = 4$, $j = 3$, and

$$\widehat{p}_4\cdot p_5 = p_4\cdot p_5 + \frac{p_2\cdot p_3}{[4|2|3\rangle}[4|5|3\rangle, \qquad (1\widehat{4}) = (14) + \frac{(2\,p_2\cdot p_3)}{[4|2|3\rangle}(13),$$
$$|\widehat{4}\rangle = |4\rangle + \frac{2\,p_2\cdot p_3}{[4|2|3\rangle}|3\rangle$$

$$M^{+----} = \frac{m\langle 5\widehat{4}\rangle[4|2|3\rangle[12][45]}{4\ [45]^2\ p_5\cdot p_1\ p_2\cdot p_3\ [34]} \tag{3.44}$$

where

$$\langle 5\widehat{4}\rangle = \langle 54\rangle + \frac{2p_2\cdot p_3}{[4|2|3\rangle}\langle 53\rangle.$$

$$M^{+-+++} = 0 \tag{3.45}$$

The amplitudes with fermion helicities $-+$ can be obtained from those above by complex conjugation. We have checked that in the soft gluon limit these results factorize as expected.

3.4.2 Results for Helicity Flip Amplitudes

We now consider the helicity flip amplitudes. These have fermion spin polarisation labels $\pm\pm$. Here we find diagrams with internal gluons, which cannot be treated with the external-spinor stripping procedure. We must therefore evaluate each side of the diagram directly, which means evaluating spinor products involving the internal momentum. Unfortunately we are unable to evaluate such products as $(\widehat{P}k)$ where k is massive. Here P is the momentum internal to the recursive diagram. In the previous section these products did not occur. Note that in the massless case round brackets do not arise, and any products $\langle\widehat{P}k\rangle$ and $[\widehat{P}k]$ can be evaluated as described in Ref. [28]. Those amplitudes in which all gluons have the same helicity do not pose a problem,

since the internal gluon diagrams vanish anyway:

$$M^{++---} = m\langle\widehat{43}\rangle \left[\frac{m(15)(42)[43] + [14](32)[\widehat{4}|1|5\rangle - [14](42)[3|1|5\rangle}{-4\ p_5\cdot p_1\ p_2\cdot p_3[34]^2[54]}\right] \tag{3.46}$$

where $i = 4$, $j = 5$ and

$$|\widehat{4}\rangle = |4\rangle + \frac{2\ p_5\cdot p_1}{[4|1|5\rangle}|5\rangle.$$

$$M^{+++++} = m[\widehat{54}] \left[\frac{m(14)(32)\langle 54\rangle + (14)\langle 42\rangle[3|2|5\rangle - (15)\langle 42\rangle[3|2|\widehat{4}\rangle}{-4\ p_5\cdot p_1\ p_2\cdot p_3\langle 45\rangle^2\langle 43\rangle}\right] \tag{3.47}$$

where $i = 3$, $j = 4$ and

$$|\widehat{4}] = |4] + \frac{2\ p_2\cdot p_3}{[3|2|4\rangle}|3].$$

We have checked that in the soft gluon limit these results factorize as expected. The amplitudes M^{--+++} and M^{-----} are obtained from those above by complex conjugation. For the remaining amplitudes we resort to Feynman diagrams.

3.5 Feynman Results

Here we give results for $\bar{q}q \to ggg$ derived from Feynman rules. Note that in a given amplitude all the helicities can be flipped by complex conjugation. In all cases where there is overlap, the following expressions agree with BCF-derived results already given.

$$
\begin{aligned}
M^{+--+-} &= -[4|2|3\rangle \left[\frac{m[14][42]\langle 53\rangle + (15)[42][4|2|3\rangle - [14](32)[4|1|5\rangle}{8\, p_5\cdot p_1\; p_2\cdot p_3\; p_3\cdot p_4\; [54]}\right] \\
&+ \langle 35\rangle \left[\frac{m[14][42]\langle 53\rangle + (15)[42][4|2|3\rangle - [14](32)[4|1|5\rangle}{8\, p_2\cdot p_3\; p_3\cdot p_4\; p_4\cdot p_5}\right] \qquad (3.48) \\
&+ \frac{\langle 35\rangle^2}{\langle 34\rangle\langle 45\rangle(p_1+p_2)^2}\left[\frac{[14](32)+(13)[42]}{[54]} + \frac{[14](52)+(15)[42]}{[34]}\right],
\end{aligned}
$$

$$
\begin{aligned}
M^{+-++-} &= -[4|1|5\rangle \left[\frac{-m(15)(52)[43] + (15)[32][4|1|5\rangle - [14](52)[3|2|5\rangle}{8\, p_5\cdot p_1\; p_2\cdot p_3\; p_4\cdot p_5\; \langle 53\rangle}\right] \\
&+ [43][4|1|5\rangle \left[\frac{[14](52) + (15)[42]}{4\, p_5\cdot p_1\; p_3\cdot p_4 \langle 53\rangle[54]}\right] \qquad (3.49) \\
&- [43]\left[\frac{[14](52)[3|1|5\rangle + (15)[32][4|1|5\rangle - m(15)(52)[43]}{4\, p_5\cdot p_1\; p_3\cdot p_4\; p_4\cdot p_5}\right] \\
&- \frac{[43]^2\langle 35\rangle}{2\, p_3\cdot p_4[54](p_1+p_2)^2}\left[\frac{[14](52) + (15)[42]}{\langle 53\rangle} + \frac{[13](52) + (15)[32]}{\langle 54\rangle]}\right],
\end{aligned}
$$

$$
\begin{aligned}
M^{+-+--} &= [3|2|4\rangle \left[\frac{m[13][32]\langle 54\rangle - [13](42)[3|1|5\rangle + (15)[32][3|2|4\rangle}{-8\, p_5\cdot p_1\; p_2\cdot p_3\; p_3\cdot p_4\; [53]}\right] \\
&+ \langle 45\rangle[3|2|4\rangle \left[\frac{[13](42) + (14)[32]}{4\, p_2\cdot p_3\; p_4\cdot p_5\langle 43\rangle[35]}\right] \qquad (3.50) \\
&+ \langle 45\rangle\left[\frac{[13](42)[3|2|5\rangle + (15)[32][3|2|4\rangle + m[13][32]\langle 54\rangle]}{8\, p_2\cdot p_3\; p_3\cdot p_4\; p_4\cdot p_5}\right] \\
&+ \frac{\langle 45\rangle^2[53]}{2\, p_4\cdot p_5\langle 43\rangle(p_1+p_2)^2}\left[\frac{[13](52) + (15)[32]}{[43]} + \frac{[13](42) + (14)[32]}{[53]}\right].
\end{aligned}
$$

The corresponding helicity flip amplitudes can be obtained from these simply by altering the types of brackets. For example, suppose we wish

to extract M^{---+-} from M^{+--+-} given above. We can achieve this by changing brackets as follows:

$$[1k] \rightarrow (1k), \tag{3.51}$$

$$(1k) \rightarrow \langle 1k\rangle, \tag{3.52}$$

where k is massless. Sandwich products such as $[4|1|5\rangle$ are not changed. This transformation results in

$$\begin{aligned} M^{---+-} &= -[4|2|3\rangle \left[\frac{m\langle 14\rangle[42]\langle 53\rangle + \langle 15\rangle[42][4|2|3\rangle - \langle 14\rangle\langle 32\rangle[4|1|5\rangle}{8\, p_5\cdot p_1\; p_2\cdot p_3\; p_3\cdot p_4\; [54]}\right] \\ &+ \langle 35\rangle\left[\frac{m\langle 14\rangle[42]\langle 53\rangle + \langle 15\rangle[42][4|2|3\rangle - \langle 14\rangle\langle 32\rangle[4|1|5\rangle}{8\, p_2\cdot p_3\; p_3\cdot p_4\; p_4\cdot p_5}\right] \\ &+ \frac{\langle 35\rangle^2}{\langle 34\rangle\langle 45\rangle(p_1+p_2)^2}\left[\frac{\langle 14\rangle\langle 32\rangle + \langle 13\rangle[42]}{[54]} + \frac{\langle 14\rangle\langle 52\rangle + \langle 15\rangle[42]}{[34]}\right]. \end{aligned} \tag{3.53}$$

Other amplitudes can be found by analogous bracket alterations.

3.6 Summary

We have calculated all the partial spin amplitudes for the $\bar{q}q \rightarrow ggg$ scattering process where q is a massive fermion. For most of the partial amplitudes we were able to use the BCFW recursion relations to obtain fairly compact expressions. This was achieved by following the idea of Ref. [32] of strip-

ping lower point amplitudes of their external fermion wavefunctions before inserting them into the recursion. We used a particular representation of massive spinors, along the lines of the Appendix of Ref. [14], to define massive spinor products. In this method information regarding the polarisation of the fermion spins is contained in the definition of the spinor products, rather than explicitly in the amplitude.

We derived new, compact results for the *helicity conserving* partial amplitudes. Their simplicity can be attributed to the vanishing of certain $2 \to 2$ scattering amplitudes, which reduces the number of contributing recursive diagrams. We were unable to treat the *helicity flip* amplitudes in the same way (except for the case where all the gluon helicities are the same), since we were unable to evaluate the corresponding recursive diagrams with internal gluons, as in such cases it is not possible to follow the external-spinor stripping procedure. For these amplitudes we instead provided expressions derived from Feynman diagrams, also in terms of massive spinor products. We have confirmed that all the results we have presented have the correct factorization properties in the soft gluon limit. Another useful check is that when the partial amplitudes are combined into a spin-summed cross-section, the result is independent of the vector k_0 used to define fermion polarisations.

These results represent an interesting test of the BCFW recursion relations [28, 30], which have not previously been applied to 5-point tree amplitudes with massive fermions. The massive spinor products we used are well suited to such calculations, though there are issues to be resolved (see

above). Application of these techniques to higher order processes with massive fermions, such as $\bar{q}q \to gggg$, should be possible though would be accompanied by an increase in complexity. This increase is, however, expected to be signficantly less than the corresponding increase in complexity using standard Feynman diagram techniques.

Chapter 4

Virtual Corrections

In this chapter we describe in some detail the calculation of the virtual corrections to gluon induced $b\bar{b}$ quark production. This amplitude is phenomenologically important for central exclusive processes, as we describe in Chapter 5. What is actually required is the amplitude

$$gg^{PP} \to b\bar{b} \tag{4.1}$$

where the PP superscript indicates that the gluons are in a $J_z = 0$, colour singlet state. We choose to work out the relevant one loop amplitude in full generality, i.e. as a vector in colour space. Only then will we apply the colour singlet operator to project onto the particular physical configuration we require. This approach facilitates comparisons with results in the literature, and could be useful for future work.

Virtual corrections to a given process basically consist of the contributions of unobserved internal particles. These necessarily form loops in the Feynman diagrams. Contrary to the situation with tree level diagrams, the presence of loops means that the momenta of each line is not determined. We must, in the spirit of quantum mechanics, integrate over all possible momenta and helicities of the internal lines.

Unfortunately, the loop integrals generally diverge in four dimensions. The divergences are of two types: *ultraviolet* (UV) and *infra-red* (IR). The UV divergences occur in the region where the loop momentum is large or, equivalentally, where the typical distance scale is small. The occurence of such poles points to a breakdown of the theory in the ultraviolet. This is hardly unexpected, as we know there must be new physics at small distance scales. If nothing else, gravitational effects must at some point become relevant. In the absence of a deeper understanding of an underlying UV-complete theory, it might appear that we can make no progress. But this is not the case. Quantum Chromodynamics is a renormalisable theory, which means we can take from experiment the short range physics that we do not understand theoretically. Renormalisation consists of admitting that the bare parameters in the Lagrangian are unphysical and divergent, and then re-expressing physical quantities in terms of other physical quantities. When we do this, there are no UV divergences. We have discussed these issues in more detail in Chapter 1.

The other class of divergences encountered in loop integrals are those

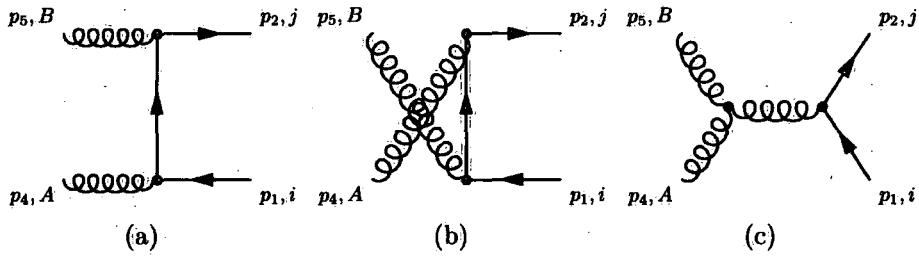

Figure 4.1: Feynman diagrams contributing to the lowest order Born amplitude. When we take the projection onto the colour singlet state gg^{PP}, the third diagram does not contribute.

in the infra-red region. These are long-distance effects, occuring when an internal particle goes on shell. They are closely related to the IR poles arising from integration over the phase space of the real contribution to the total cross section. In fact, as was discussed in the introduction, for well defined observables the IR poles are required to cancel between the real and virtual contributions by the KLN theorem [5].

For the processes considered in this thesis the virtual parts are simply $2 \to 2$ scattering amplitudes. The loop amplitudes contribute to the NLO part of the total cross section. They are added coherently to the Born amplitudes, and then squared. Consequently it is the interference term $2\,\Re e(M^*_{born} M_{loop})$ that we are interested in. The relevant Feynman diagrams are shown at tree level in Fig. 4.1 and at one loop in Fig. 4.2.

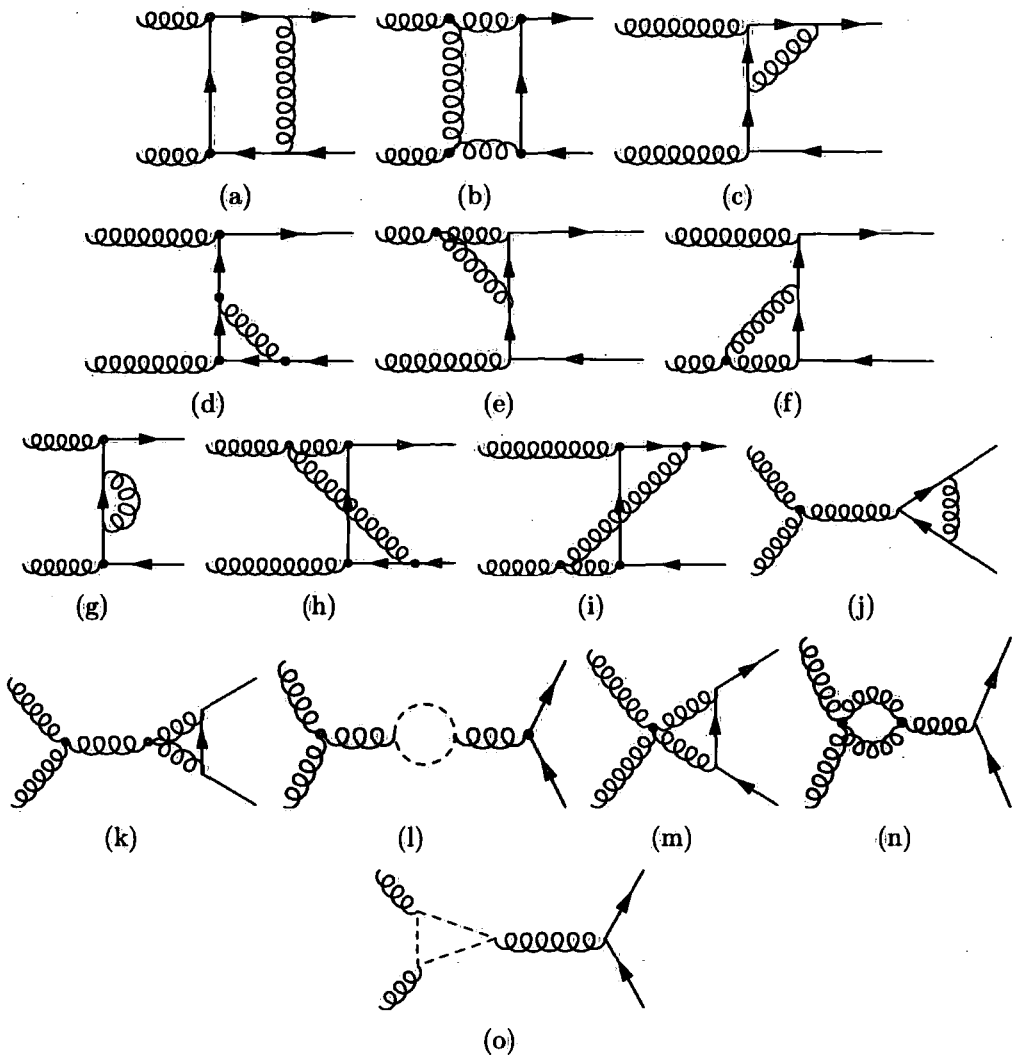

Figure 4.2: One-loop Feynman diagrams contributing to the process $gg \to b\bar{b}$. Dashes indicate gluon, quark and ghost loops. There are an additional seven graphs corresponding to switching the external gluons of graphs (a) through (g) above.

4.0.1 Dimensional Regularisation

Let us examine a typical loop integal.

$$I = \int \frac{d^4k}{k^2[(k+p)^2 - m^2]}. \tag{4.2}$$

Here k is the loop momentum and p is the momentum of one of the external partons, or a sum of such momenta. This is a scalar loop integral, so called because the numerator does not contain any free Lorentz indices associated with the integration momentum. By simply counting powers of k we can see that the above integral will be logarithmically divergent. If we regulate the integral by imposing an upper cut off on k, then we find

$$I \to \int^{\Gamma} \frac{\mathrm{d}k}{k} \to \ln(\Gamma). \tag{4.3}$$

We call this an ultraviolet (UV) divergence because it is the high momentum part of the integration region which leads to the pole. In practical applications the above regularisation is not particularly useful because it violates Lorentz invariance. Dimensional regularisation is almost universally preferred, as it has the virtue of respecting the symmetries present in the theory. It involves redefining the theory to take place in $d = 4 - 2\epsilon$ dimensions. The loop integrals are then finite, but contain poles in ϵ.

Scalar loop integrals can be classified according to the number of factors in the denominator. The integral in (4.2) is called a two point integral, and

we will also encounter three- and four-point integrals. These objects can be straightforwardly evaluated, and expressions for them are available in the literature. We define,

$$
\begin{aligned}
A_0(m) &= \int \frac{d^dk}{(2\pi)^d} \frac{1}{k^2 - m^2}, \\
B_0(p, m_1, m_2) &= \int \frac{d^dk}{(2\pi)^d} \frac{1}{[k^2 - m_1^2][(k+p_1)^2 - m_2^2]}, \\
C_0(p_1, p_2, m_1, m_2, m_3) &= \int \frac{d^dk}{(2\pi)^d} \frac{1}{[k^2 - m_1^2][(k+p_1)^2 - m_2^2][(k+p_{12})^2 - m_3^2]}, \\
D_0(p_1, p_2, p_3, m_1, m_2, m_3, m_4) &= \\
&\int \frac{d^dk}{(2\pi)^d} \frac{1}{[k^2 - m_1^2][(k+p_1)^2 - m_2^2][(k+p_{12})^2 - m_3^2][(k+p_{123} - m_4^2]}.
\end{aligned}
\tag{4.4}
$$

Here we have used the shorthand notation $p_{i\ldots k} = p_i + \cdots + p_k$. Analytic expressions for these integrals can be found in, for example [43].

4.0.2 Reduction of Tensor Integrals

In the analytical expression of a given Feynman diagram there are also *tensor* integrals. These have a tensor structure in the numerator involving the loop momentum k. Of course, since an amplitude is a scalar object, these tensors will ultimately be contracted with one of the external momenta p_i or polarisation vectors ϵ_i.

The tensor integrals can be expressed in terms of scalar integrals. There are many procedures for achieving this. We will use the original method, first outlined by Passarino and Veltman in [44]. Let us take as an example

the three-point tensor integral

$$I^{\mu\nu} = \int d^d k \, \frac{k^\mu k^\nu}{[k^2 - m_1^2]\,[(k+p_1)^2 - m_2^2]\,[(k+p_1+p_2)^2 - m_3^2]}. \tag{4.5}$$

The idea is to use Lorentz invariance to express $I^{\mu\nu}$ as a sum of terms, each proportional to one of the possible tensor structures. Thus we write,

$$I^{\mu\nu} = C_{21}\, p_1^\mu p_1^\nu + C_{22}\, p_2^\mu p_2^\nu + C_{23}\, \{p_1^\mu p_2^\nu\} + C_{24}\, g_{\mu\nu}, \tag{4.6}$$

where $\{p_1^\mu p_2^\nu\} = p_1^\mu p_2^\nu + p_2^\mu p_1^\nu$. We now solve for the unknown coefficients by contracting $I_{\mu\nu}$ with the various external momenta and the metric tensor. On the RHS we then have terms such as $k \cdot p_1$, which are re-written in terms of one or more of the factors appearing in the denominator. For example,

$$2k \cdot p_1 = [(k+p_1)^2 - m_2^2] - [k^2 - m_1^2] + [m_2^2 - m_1^2 - p_1^2]. \tag{4.7}$$

The first two terms above allow a cancellation between numerator and denominator, thus reducing these terms to lower point integrals. The last term no longer contains the loop momentum, so that the rank of the tensor in the numerator is reduced by one. The next step is to solve the resulting set of simultaneous equations for the unknown coefficients. This is done for all the cases we need in Appendix A.

4.0.3 The Calculation

The virtual corrections to the Born level partonic process $gg^{PP} \rightarrow b\bar{b}$ consist of bubble, triangle and box loop integrals. A full list of diagrams is given in Fig. (4.2). Each diagram contains a tensor loop integral. Since these integrals are in general divergent, both in the UV and IR regions, we regulate them by working in $d = 4 - 2\epsilon$ dimensions. These integrals are written as sums of scalar integrals multiplied by tensors independent of the loop momentum and the metric tensor, as per the usual Passarino-Veltman reduction scheme. The momenta are labelled as

$$g^A(p_4)\ g^B(p_5) \longrightarrow \bar{b}_i(p_1)\ b_j(p_2) \tag{4.8}$$

We then express the amplitude as a linear combination of twenty Dirac structures, each with a coefficient K_{ij},

$$M^{virt} = \sum_{i=1}^{3} \sum_{j=1}^{20} C_i\ K_{ij}\ T_j. \tag{4.9}$$

The C_i are the fundamental colour structures. There are only three of these, given by

$$C_1 = (t^A\ t^B)_{ij}, \qquad C_2 = (t^B\ t^A)_{ij}, \qquad C_3 = \delta^{AB}\delta_{ij}. \tag{4.10}$$

The Dirac structures we have used are:

$$
\begin{aligned}
T_1 &= \overline{u}(p_1)v(p_2)\ \epsilon(p_4)\cdot p_1\ \epsilon(p_5)\cdot p_1 \\
T_2 &= \overline{u}(p_1)v(p_2)\ \epsilon(p_4)\cdot p_1\ \epsilon(p_5)\cdot p_2 \\
T_3 &= \overline{u}(p_1)v(p_2)\ \epsilon(p_4)\cdot p_2\ \epsilon(p_5)\cdot p_1 \\
T_4 &= \overline{u}(p_1)v(p_2)\ \epsilon(p_4)\cdot p_2\ \epsilon(p_5)\cdot p_2 \\
T_5 &= \overline{u}(p_1)\not{p}_4 v(p_2)\ \epsilon(p_4)\cdot p_1\ \epsilon(p_5)\cdot p_1 \\
T_6 &= \overline{u}(p_1)\not{p}_4 v(p_2)\ \epsilon(p_4)\cdot p_1\ \epsilon(p_5)\cdot p_2 \\
T_7 &= \overline{u}(p_1)\not{p}_4 v(p_2)\ \epsilon(p_4)\cdot p_2\ \epsilon(p_5)\cdot p_1 \\
T_8 &= \overline{u}(p_1)\not{p}_4 v(p_2)\ \epsilon(p_4)\cdot p_2\ \epsilon(p_5)\cdot p_2 \\
T_9 &= \overline{u}(p_1)\not{\epsilon}_4 v(p_2)\ \epsilon(p_5)\cdot p_1 \\
T_{10} &= \overline{u}(p_1)\not{\epsilon}_4 v(p_2)\ \epsilon(p_5)\cdot p_2 \\
T_{11} &= \overline{u}(p_1)\not{\epsilon}_5 v(p_2)\ \epsilon(p_4)\cdot p_1 \\
T_{12} &= \overline{u}(p_1)\not{\epsilon}_5 v(p_2)\ \epsilon(p_4)\cdot p_2 \\
T_{13} &= \overline{u}(p_1)\not{\epsilon}_4\ \not{p}_4 v(p_2)\ \epsilon(p_5)\cdot p_1 \\
T_{14} &= \overline{u}(p_1)\not{\epsilon}_4\ \not{p}_4 v(p_2)\ \epsilon(p_5)\cdot p_2 \\
T_{15} &= \overline{u}(p_1)\not{\epsilon}_5\ \not{p}_5 v(p_2)\ \epsilon(p_4)\cdot p_1 \\
T_{16} &= \overline{u}(p_1)\not{\epsilon}_5\ \not{p}_5 v(p_2)\ \epsilon(p_4)\cdot p_2 \\
T_{17} &= \overline{u}(p_1)\not{\epsilon}_5\ \not{\epsilon}_4 v(p_2) \\
T_{18} &= \overline{u}(p_1)\not{\epsilon}_4\ \not{\epsilon}_5 v(p_2) \\
T_{19} &= \overline{u}(p_1)\ \not{\epsilon}_4\ \not{p}_4\ \not{\epsilon}_5\ v(p_2) \\
T_{20} &= \overline{u}(p_1)\ \not{\epsilon}_5\ \not{p}_4\ \not{\epsilon}_4\ v(p_2)
\end{aligned}
$$

Since there are three colour structures and twenty Dirac structures, this means there are sixty components K_{ij}. Each of these will depend on kinematical invariants $s_{ij} = 2\ p_i \cdot p_j$ and the mass m. All the information associated with the external wavefunctions, i.e. the spinors and polarisation vectors, is contained in the T_i. This means that the K_{ij} coefficients do not depend on the helicity configuration. We can evaluate them once and for all, and then construct the polarised $J_z = 0$ state we require numerically, simply by summing over those configurations in which the gluons have the same helicity.

Gauge invariance places conditions on the coefficients in Eq.(4.9). Gauge invariance can be expressed in terms of the Ward identity, which says that if we replace a polarisation vector with its associated momentum, then the amplitude vanishes. When we impose this for each of the intitial state gluons, we can derive a system of ten simultaneous equations relating the coefficients of the twenty Dirac structures. Solving this system enables us to halve the number of coefficients needed to expand the amplitude as in (4.9). We choose instead to keep the full set of coefficients, and use gauge invariance as a check of the calculation. That is to say, once we have evaluated the K_{ij} we can check that they collectively satisfy the requirements imposed by gauge invariance. This is a very strong check on the calculation.

Beginning with general expressions for each of the Feynman diagrams in Fig. 4.2 we used the algebraic manipulation tool FORM [45] to transform the amplitude into the form of Eq.(4.9) and implement the Passarino-Veltman

reduction of tensor integrals into scalar integrals. The scalar integrals are all known and are given in, for example [43]. The output of the FORM program is a series of expressions for the coefficients K_{ij}. These serve as input to a FORTRAN numerical program. The expressions for the coefficients are too large to be presented here, but can be obtained on request from the author. By way of example, we give here the corresponding coefficients for the tree amplitude,

$$K_{1,11} = -\frac{2}{s_{14}} - \frac{2}{s_{45}}, \tag{4.11}$$

$$K_{2,11} = \frac{2}{s_{45}}, \tag{4.12}$$

$$K_{1,12} = -\frac{2}{s_{45}}, \tag{4.13}$$

$$K_{2,12} = \frac{2}{s_{15}} + \frac{2}{s_{45}}, \tag{4.14}$$

$$K_{1,19} = -\frac{1}{s_{14}} - \frac{1}{s_{45}}, \tag{4.15}$$

$$K_{2,19} = \frac{1}{s_{45}}, \tag{4.16}$$

$$K_{1,20} = -\frac{1}{s_{45}}, \tag{4.17}$$

$$K_{2,20} = \frac{1}{s_{15}} + \frac{1}{s_{45}}, \tag{4.18}$$

with all the other coefficients zero. We see that at tree level the third colour structure δ_{AB} does not contribute.

4.1 Checks

Obviously for such a large and intricate calculation as this it is important to have available a range of consistency checks on the final answer. There are a few ways in which we can verify that everything has worked correctly. Firstly, there is the pole structure. Recall that the loop amplitude is divergent in 4 dimensions, which is why we regulated it by working in $d = 4 - 2\epsilon$ dimensions. The divergences then manifest themselves as poles in epsilon. The UV divergences appear as single poles $(1/\epsilon)$, while the IR divergences appear as both single and double $(1/\epsilon^2)$ poles. The structure of these singularities is predictable. That is to say, one may check the precise coefficients of the poles obtained and determine if they are in accordance with what is expected. Catani et al. [46] have presented the expected structure in full generality. Their results were obtained by direct integration of real amplitudes squared, which are related through the KLN theorem to the poles of certain loop amplitudes. We present the particular result for $gg \to \bar{b}b$ here for convenience[1]. The pole structure is obtained by operating on the colour vector representing the tree level amplitude with a 3×3 matrix,

$$M^{\text{1-loop}}|_{\epsilon,\epsilon^2} = \frac{(4\pi)^\epsilon}{\Gamma(1-\epsilon)}\left(\frac{X}{\epsilon^2} + \frac{Y}{\epsilon}\right) M^{\text{tree}}. \tag{4.19}$$

[1]In [46] the general expression for the pole structure was presented in a different notation.

Here each side of the equation is understood to be a vector in colour space, i.e. a column vector where the elements are the coefficients of the three colour structures given in Eq. (4.10). The matrices X and Y can be derived from the results of [46].

The double pole part, described by X, turns out to be diagonal in the colour space,

$$X = -2N \begin{pmatrix} 1 & 0 & 0 \\ 0 & 1 & 0 \\ 0 & 0 & 1 \end{pmatrix}. \tag{4.20}$$

Another way of saying this is that the $(1/\epsilon^2)$ part of the loop amplitude is proportional the tree level amplitude, with the constant of proportionality $-2N$. The single pole parts are more complicated. We find,

$$Y = \begin{pmatrix} Y_{11} & 0 & Y_{13} \\ 0 & Y_{22} & Y_{23} \\ Y_{13} & Y_{23} & Y_{33} \end{pmatrix} \tag{4.21}$$

where

$$
\begin{aligned}
Y_{11} &= \frac{(s_{45}-2m^2)}{Ns\beta}\ln x - N\ln\left(\frac{\mu^2}{s_{45}}\right) - N\ln\left(\frac{\mu^2}{s_{14}}\right) - N\ln\left(\frac{m^2}{s_{14}}\right) \\
&\quad - 2\left(C_F + \frac{11C_A}{6}\right) \\
Y_{22} &= Y_{11}\Big|_{s_{14}\leftrightarrow s_{15}} \\
Y_{33} &= \frac{2C_F(s_{45}-2m^2)}{s\beta}\ln x - 4C_F\ln\left(\frac{m^2}{s_{15}}\right) - \frac{2}{N}\ln\left(\frac{\mu^2}{s_{45}}\right) \\
&\quad - 2\left(C_F + \frac{11C_A}{6}\right) \\
Y_{13} &= \frac{(s_{45}-2m^2)}{s\beta}\ln x + N\ln\left(\frac{\mu^2}{s_{15}}\right) - N\ln\left(\frac{\mu^2}{s_{45}}\right) + N\ln\left(\frac{\mu^2}{s_{15}}\right) \\
Y_{23} &= Y_{13}\Big|_{s_{14}\leftrightarrow s_{15}},
\end{aligned}
$$

where $\beta = \sqrt{1-4m^2/s_{45}}$. We have checked that the pole structure we obtain is precisely that predicted in [46].

As mentioned in the preview subsection, another strong check is based on gauge invariance. We can express gauge invariance as a set of equations which must be obeyed by the coefficients K_{ij}. These equations are derived by imposing the Ward identity on the general expression Eq.(4.9). We obtain

the following set of equations:

$$
\begin{aligned}
0 &= K_{i1}\, s_{14} + K_{i3}\, s_{15} - 4K_{i17}, \\
0 &= K_{i2}\, s_{14} + K_{i4}\, s_{15} - 4K_{i18}, \\
0 &= K_{i5}\, s_{14} + K_{i7}\, s_{15} + 2K_{i9}, \\
0 &= K_{i6}\, s_{14} + K_{i8}\, s_{15} + 2K_{i10}, \\
0 &= K_{i11}\, s_{14} + K_{i12}\, s_{15} + 4mK_{i17} - 4mK_{i18}, \\
0 &= K_{i15}\, s_{14} + K_{i16}\, s_{15} - 2K_{i17} + 2K_{i18}, \\
0 &= K_{i1}\, s_{15} + K_{i2}\, s_{14} - 4K_{i18}, \\
0 &= K_{i3}\, s_{15} + K_{i4}\, s_{14} - 4K_{i17}, \\
0 &= K_{i5}\, s_{15} + K_{i6}\, s_{14} - 2K_{i11} + 4K_{i19}, \\
0 &= K_{i7}\, s_{15} + K_{i8}\, s_{14} - 2K_{i12} + 4K_{i20}, \\
0 &= K_{i9}\, s_{15} + K_{i10}\, s_{14} - 4mK_{i17} + 4mK_{i18} - 2s_{14}\, K_{i19} - 2s_{15}\, K_{i20}, \\
0 &= K_{i13}\, s_{15} + K_{i14}\, s_{14} - 2K_{i18} + 2K_{i17}.
\end{aligned}
$$

Notice that the first index of the coefficient is free - this is the colour index. The above conditions hold for each of the three colour structures. We have checked numerically that our results are gauge invariant in the manner described above.

A third check is provided by the over-determination of the Passarino-Veltman reduction coefficients. Some of the tensor integral reduction formulae can be solved in more than one way, giving several different, though

equivalent, expressions. One should obtain the same results using either expression. This is a strong check that the tensor reduction has been performed correctly.

Finally, we have checked our results against a similar calculation described in [47]. The authors of that paper used a different set of Dirac structures to ours, and present diagram by diagram results. We have verified numerically that the two sets of coefficients are fully equivalent.

Chapter 5

Central Exclusive Production

In this chapter we describe central exclusive production and why it is interesting. We also explain how the results presented thus far in this thesis find application in the consideration of NLO backgrounds to Higgs production.

Determining the precise mechanism of electroweak symmetry breaking is perhaps the most pressing concern in particle physics today. The Large Hadron Collider (LHC), due to come online within a few months, is designed with this in mind. Its two main detectors, ATLAS and CMS, will search for signatures of the Higgs boson, thought to be responsible for spontaneously breaking the electroweak symmetry of the standard model. The LEP collider, while failing to directly observe the Higgs, did enable a lower bound of 114 GeV to be placed on its mass [48]. Meanwhile, the consideration of electroweak processes to which virtual Higgs particles would be expected to contribute, suggests [49] that the Higgs is light - in the range 87^{+36}_{-27} GeV.

The focus to date has primarily been on inclusive production, in which the two incident protons each contribute one parton to the hard scattering, and then disassociate into unobserved remnants. However, exclusive production modes offer a range of advantages (and present some difficulties) and should not be overlooked in the search for new physics. There has been much interest in Central Exclusive Production (CEP) [50–53], in which each proton is required to remain intact, and is observed in the final state. In this way, a central resonance may be produced. If the protons are observed at small angular deviations, this resonance must be formed in a $J_z = 0$ state.[1] It is also easy to see that the resonance is required to be a colour-singlet, with $CP = 1$. The consideration of such processes has led to a proposal [54, 55] to complement the ATLAS and CMS detectors at the LHC with forward proton detectors, which would be installed 420m from the interaction region.

We denote the basic process by $pp \to p \oplus X \oplus p$. Here the $\oplus$ signs represent an absence of hadronic activity between the two observed outgoing protons and the centrally produced resonance X. This reflects the especially clean final state configurations. Since the protons are colourless objects, they must exchange at least two gluons in this process. The centrally produced resonance X can be anything in a $J_z = 0$ state and with the appropriate quantum numbers, as discussed above. Perhaps the most interesting situation is the formation of a Higgs boson, as illustrated in Fig. (5.1). The primary advantages of this arrangement are as follows.

[1]Here J_z refers to the projection of the angular momentum onto the z axis.

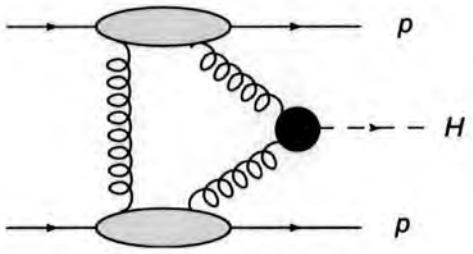

Figure 5.1: A sketch of the basic mechanism of central exclusive Higgs production. The Higgs is produced via a top loop arising from the fusion of the active gluon pair. The screening gluon on the left ensures colour conservation.

- Firstly, the $J_z = 0$ selection rule eliminates a large portion of the QCD background, which is predominantly $b\bar{b}$ production and mainly proceeds through the $J_z = 2$ state. The leading order background is mass-suppressed. For massless quarks it vanishes, and when the mass of the b quark is retained we find an $\mathcal{O}(m^2/s)$ dependence, at least at large angles. The amplitude has terms such as

$$\frac{m^2}{E^2}\frac{1}{1-\beta\cos\theta}, \tag{5.1}$$

where $\beta = (1 - m^2/E^2)^{1/2}$. For large angle scattering we see clearly the $\mathcal{O}(m^2/s)$ behaviour mentioned above. For $m \ll E$ we can expand the square root in the definition of β as $1 - m^2/2E^2$, while for small angles the cosine can be approximated as $1 - \theta^2/2$. In this limit the term above tends to

$$\frac{2m^2}{E^2}\frac{1}{(m/E)^2+\theta^2}. \tag{5.2}$$

We can see now that for very small angle scattering the theta term can

be ignored and the expression is of order unity. However, in reality we always impose an experimental cut on the angle θ, or equivalently on the transverse momentum of the final state partons, thus avoiding the behaviour described above.

- Second, by observing the final state protons and measuring their momenta, we can infer the mass of the resonance using simple momentum conservation. This is impossible in an inclusive situation, because in this case the proton remnants go undetected down the beam pipe. This indirect measurement would typically be much more accurate than one obtained from direct observation of the decay products of X. If X is, for example, a light Higgs boson[2], then it will decay predominantly to a pair of b jets. The branching ratio of Higgs decays is shown in Fig. 5.2. Measuring the energy of jets is in general a rather inexact business, so the availability of an indirect method to measure the energy of the central resonance is extremely useful. In this way accuracies of $\mathcal{O}(1\%)$ can be achieved.

- Ordinarily the Higgs decays to fermions (such as b quarks) are difficult to observe experimentally due to the large QCD backgrounds. This is why focus has turned to the $\gamma\gamma$ channel to search for a light Higgs, even though the branching ratio for this decay is quite small. The background problem is alleviated in central exclusive searches due to

[2]Unless stated otherwise, by 'Higgs boson' we mean a standard model Higgs.

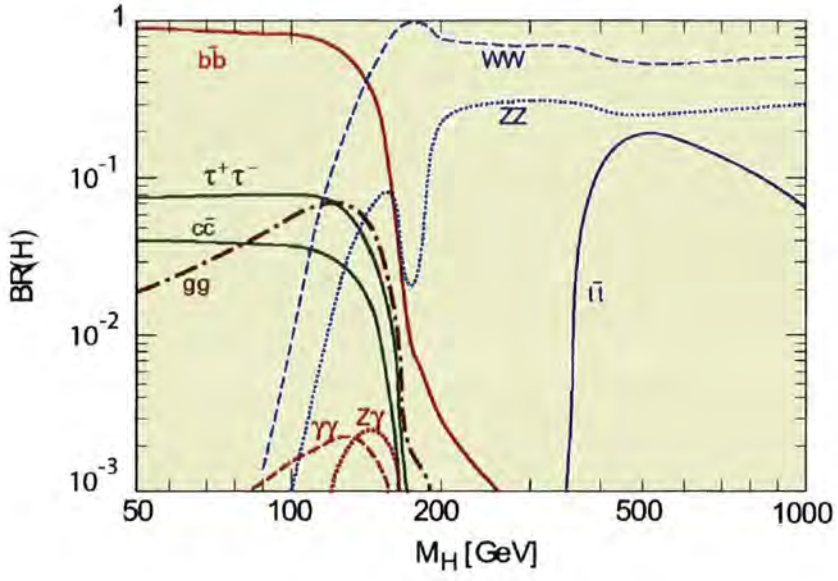

Figure 5.2: The branching ratios of the decay of a standard model Higgs boson. In the light region, $M_H \lesssim 150$ GeV the Higgs decays mainly into $b\bar{b}$.

the $J_z = 0$ selection rule, so that the Higgs coupling to fermions can be more easily studied.

- Lastly, from the mere observation of a resonance produced in this way, one can deduce that the C and the P quantum numbers are $+1$. We recall here that in the MSSM the various Higgs particles have different C and P quantum numbers. In inclusive searches, it is difficult at a hadron collider to get information on the CP structure. One would ideally need a lepton collider for this purpose.

The only irreducible background to central exclusive production of a light Higgs boson, which is expected to decay mainly into two b-jets, is the direct

production of two b-jets via the same mechanism. We can write this as

$$pp \to p \oplus gg^{PP} \to b\,\bar{b} \oplus p, \tag{5.3}$$

where the PP superscript indicates that the gluons are in a $J_z = 0$, colour-singlet state. This background was considered in Refs. [52, 56–58]. In the approximation that the outgoing protons have vanishing transverse momentum, the leading order background is suppressed by a $J_z = 0$ selection rule. It vanishes for massless quarks and is $\mathcal{O}(m^2)$ when the b quark mass is retained, neglecting end effects[3]. The NLO corrections consist of virtual diagrams contributing to the $gg^{PP} \to b\bar{b}$ process and the real emission of an extra gluon in the final state, $gg^{PP} \to b\bar{b}g$. These processes are not expected to be mass suppressed, and so we can expect large corrections at NLO.

We therefore see that both the real emission (Chapter 3) and loop (Chapter 4) amplitudes presented in this thesis are necessary inputs to a NLO calculation of the dijet background, as described above.

[3]For $\theta \gtrsim m/E$ the amplitude squared is $\mathcal{O}(m^2)$, but for $\theta \lesssim m/E$ we find it to be $\mathcal{O}(1)$.

Chapter 6

Summary

In Chapters 2 and 3 we built on the twistor space inspired methods introduced in [22] and [28]. These new techniques can be broadly classified as *on shell* methods. The familiar Feynman diagram expansion uses off shell objects as building blocks. In contrast, the MHV rules and BCF recursion relations use on shell lower point amplitudes. This setup has the advantage that work performed in calculating and simplifying the lower point amplitudes does not have to be repeated - they are simply fed in to the new calculation. Also, the use of scalar, gauge invariant objects means the resulting diagrams are simple - there are no spinor or Lorentz indices. We applied both the new techniques to QED amplitudes, and showed that simple expressions for helicity amplitudes can be easily obtained. We then turned our attention to amplitudes involving massive fermions. In the original papers [22,28] fermion masses were not included. We built on the work of [31,32] to calculate the 5

parton amplitudes $gg \to b\bar{b}g$.

Central Exclusive Production (CEP) is an interesting alternative to traditional avenues for searching for new physics. There are various advantages to Higgs boson searches in this channel, one such being the leading order suppression of the dijet background to $H \to b\bar{b}$. However at NLO there is no such suppression, and so it is important to ascertain by calculation the size of the NLO corrections. In Chapter 3 we evaluated the real emission amplitudes needed for such a calculation, and then in Chapter 4 we presented the loop amplitude which is responsible for the virtual corrections at next to leading order. Chapter 5 consisted of a detailed description of this production mechanism, and of the relevance or our results.

Appendix A

Passarino Veltman Decomposition

In this appendix we describe the reduction of tensor loop integrals. The basic procedure was outlined in Chapter 4. Here we present expressions for all the coefficients. Formulae for the scalar integrals A_0, B_0, C_0 and D_0 can be found elsewhere, for example [43].

A.1 Bubbles

The bubbles are defined as

$$B_0; B^\mu; B^{\mu\nu}(p, m_1, m_2) = \int \frac{d^d k}{(2\pi)^d} \frac{1; k^\mu; k^{\mu\nu}}{[k^2 - m_1^2]\,[(k+p)^2 - m_2^2]}.$$

We do not encounter higher ranks than 2 in the case of bubbles. We expand the tensor integrals as follows,

$$\begin{aligned} B^{\mu}(p, m_1, m_2) &= p^{\mu} B_1, \\ B^{\mu\nu}(p, m_1, m_2) &= p^{\mu} p^{\nu} B_{21} + g^{\mu\nu} B_{22}. \end{aligned}$$

We have omitted the arguments of the form factors for clarity. They depend on all possible scalar invariants of the leg momenta and masses. The curly bracket $\{\dots\}$ construction is a convenient shorthand for representing the sum of all possible permutations of different Lorentz indices. So for example $\{p_1, p_2\}^{\mu\nu} = p_1^{\mu} p_2^{\nu} + p_1^{\mu} p_2^{\nu}$.

We find

$$B_1 = \frac{1}{2p^2}\left[A(m_1) - A(m_2) + (m_2^2 - m_1^2 - p^2) B_0\right] \tag{A.1}$$

$$B_{22} = \frac{R_{02} - R_{01}}{d-1} \tag{A.2}$$

$$B_{21} = \frac{R_{01} - B_{22}}{p^2}. \tag{A.3}$$

with

$$R_{01} = f B_1/2 + A(m_2)/2, \tag{A.4}$$

$$R_{02} = A(m_2) + m_1^2 B_0, \tag{A.5}$$

$$f = m_2^2 - m_1^2 - p^2. \tag{A.6}$$

A.2 Triangles

We will encounter the following tensor triangle integrals,

$$C_0; C^\mu; C^{\mu\nu}; C^{\mu\nu\rho}(p_1, p_2, m_1, m_2, m_3) = \int \frac{d^d k}{(2\pi)^d} \frac{1; k^\mu; k^{\mu\nu}; k^{\mu\nu\rho}}{[k^2 - m_1^2]\,[(k+p_1)^2 - m_2^2]\,[(k+p_{12})^2 - m_3^2]}.$$

By Lorentz symmetry, we can express a given tensor integral as a sum of form factors multiplied by tensors composed of the leg momenta and metric. Following [44], we define

$$\begin{aligned}
C^\mu &= p_1^\mu C_1 + p_2^\mu C_2, \\
C^{\mu\nu} &= p_1^\mu p_2^\nu C_{21} + p_2^\mu p_1^\nu C_{22} + \{p_1, p_2\}^{\mu\nu} C_{23} + g^{\mu\nu} C_{24}, \\
C^{\mu\nu\rho} &= p_1^\mu p_1^\nu p_1^\rho C_{31} + p_2^\mu p_2^\nu p_2^\rho C_{32} \\
&+ \{p_2, p_1, p_1\}^{\mu\nu\rho} C_{33} + \{p_1, p_2, p_2\}^{\mu\nu\rho} C_{34} \\
&+ \{p_1, g\}^{\mu\nu\rho} C_{35} + \{p_2, g\}^{\mu\nu\rho} C_{36}.
\end{aligned}$$

As described in Chapter 4, by contracting the various tensor integrals with leg momenta and the metric tensor we can obtain a system of simultaneous equations, which can then be solved for the form factors. The results are as

follows:

$$
\begin{aligned}
f_1 &= m_2^2 - m_1^2 - p_1^2 \\
f_2 &= m_3^2 - m_2^2 - p_5^2 + p_1^2 \\
C_{24} &= \frac{1}{(d-2)}[-m_1^2 C_0 + (B_0(p_2, m_2, m_3) - f_1 C_{11} - f_2 C_{12})/2] \\
R_1 &= \frac{1}{2}[f_1 C_0 + B_0(p_5, m_1, m_3) - B_0(p_2, m_2, m_3)] \\
R_2 &= \frac{1}{2}[f_2 C_0 + B_0(p_1, m_1, m_2) - B_0(p_5, m_1, m_3)] \\
R_3 &= \frac{1}{2}[f_1 C_{11} + B_1(p_5, m_1, m_3) + B_0(p_2, m_2, m_3)] - C_{24} \\
R_4 &= \frac{1}{2}[f_1 C_{12} + B_1(p_5, m_1, m_3) - B_1(p_2, m_2, m_3)] \\
R_5 &= \frac{1}{2}[f_2 C_{11} + B_1(p_1, m_1, m_2) - B_1(p_5, m_1, m_3)] \\
R_6 &= \frac{1}{2}[f_2 C_{12} - B_1(p_5, m_1, m_3)] - C_{24}
\end{aligned}
$$

$$
G_2 = \begin{pmatrix} p_1^2 & p_1 \cdot p_2 \\ p_2 \cdot p_1 & p_2^2 \end{pmatrix}
$$

$$
\begin{pmatrix} C_{11} \\ C_{12} \end{pmatrix} = G_2^{-1} \begin{pmatrix} R_1 \\ R_2 \end{pmatrix}
$$

$$
\begin{pmatrix} C_{23} \\ C_{22} \end{pmatrix} = G_2^{-1} \begin{pmatrix} R_4 \\ R_6 \end{pmatrix}
$$

$$
\begin{pmatrix} C_{21} \\ C_{23} \end{pmatrix} = G_2^{-1} \begin{pmatrix} R_3 \\ R_5 \end{pmatrix}
$$

Here G_2 is a Gram matrix which arises in solving for the form factors. One of the disadvantages of this method of tensor integral reduction is that for certain configurations of external momenta the inverse of the Gram matrix diverges. We then find large cancellations between different parts of the calculation. While this wouldn't be problem for an entirely analytical calculation, in practise we always run simulations numerically and the large cancellations can affect accuracy. For the processes considered in this thesis this effect is relatively harmless, but it is a problem for calculations with more external partons . Fortunately there are numerous other techniques for tensor integral reduction which avoid this issue, and the reader is directed to [59] for a review of these.

$$
\begin{aligned}
R_{11} &= \frac{1}{2}[f_1 C_{24} + B_{22}(p_5, m_1, m_3) - B_{22}(p_2, m_2, m_3)] \\
R_{15} &= \frac{1}{2}[f_2 C_{24} + B_{22}(p_1, m_1, m_2) - B_{22}(p_5, m_1, m_3)] \\
R_8 &= \frac{1}{2}[f_1 C_{21} + B_{21}(p_5, m_1, m_3) - B_0(p_2, m_2, m_3)] - 2C_{35} \\
R_9 &= \frac{1}{2}[f_1 C_{22} + B_{21}(p_5, m_1, m_3) - B_{21}(p_2, m_2, m_3)] \\
R_{10} &= \frac{1}{2}[f_1 C_{23} + B_{21}(p_1, m_1, m_3) + B_1(p_2, m_2, m_3)] - C_{36} \\
R_{12} &= \frac{1}{2}[f_2 C_{21} + B_{21}(p_1, m_1, m_2) - B_{21}(p_5, m_1, m_3)] \\
R_{13} &= \frac{1}{2}[f_2 C_{22} - B_{21}(p_5, m_1, m_3)] - 2C_{36} \\
R_{14} &= \frac{1}{2}[f_2 C_{23} - B_{21}(p_5, m_1, m_3)] - C_{35}
\end{aligned}
$$

$$\begin{pmatrix} C_{35} \\ C_{36} \end{pmatrix} = G_2^{-1} \begin{pmatrix} R_{11} \\ R_{15} \end{pmatrix},$$

$$\begin{pmatrix} C_{33} \\ C_{34} \end{pmatrix} = G_2^{-1} \begin{pmatrix} R_{10} \\ R_{14} \end{pmatrix},$$

$$\begin{pmatrix} C_{31} \\ C_{33} \end{pmatrix} = G_2^{-1} \begin{pmatrix} R_{8} \\ R_{12} \end{pmatrix},$$

$$\begin{pmatrix} C_{34} \\ C_{32} \end{pmatrix} = G_2^{-1} \begin{pmatrix} R_{9} \\ R_{5} \end{pmatrix}.$$

A.3 Boxes

For the boxes matters proceed similarly as for the triangles. We make the following definition,

$$D_0; D^{\mu}; D^{\mu\nu}; D^{\mu\nu\rho}, D^{\mu\nu\rho\sigma}(p_1, p_2, p_3, m_1, m_2, m_3, m_4) =$$

$$\int \frac{d^d k}{(2\pi)^d} \frac{1; k^{\mu}; k^{\mu\nu}; k^{\mu\nu\rho}; k^{\mu\nu\rho\sigma}}{[k^2 - m_1^2][(k+p_1)^2 - m_2^2][(k+p_{12})^2 - m_3^2][(k+p_{123})^2 - m_4^2]},$$

$$
\begin{aligned}
D^{\mu} &= p_1^{\mu} D_{11} + p_2^{\mu} D_{12} + p_3^{\mu} D_{13} \\
D^{\mu\nu} &= p_1^{\mu} p_1^{\nu} D_{21} + p_2^{\mu} p_2^{\nu} D_{22} + p_3^{\mu} p_3^{\nu} D_{23} \\
&+ \{p_1, p_2\}^{\mu\nu} D_{24} + \{p_1, p_3\}^{\mu\nu} D_{25} + \{p_2, p_3\}^{\mu\nu} D_{26} + g^{\mu\nu} D_{27} \\
D^{\mu\nu\rho} &= p_1^{\mu} p_1^{\nu} p_1^{\rho} D_{31} + p_2^{\mu} p_2^{\nu} p_2^{\rho} D_{32} + p_3^{\mu} p_3^{\nu} p_3^{\rho} D_{33} \\
&+ \{p_2, p_1, p_1\}^{\mu\nu\rho} D_{34} + \{p_3, p_1, p_1\}^{\mu\nu\rho} D_{35} + \{p_1, p_2, p_2\}^{\mu\nu\rho} D_{36} \\
&+ \{p_1, p_3, p_3\}^{\mu\nu\rho} D_{37} + \{p_3, p_2, p_2\}^{\mu\nu\rho} D_{38} + \{p_2, p_3, p_3\}^{\mu\nu\rho} D_{39} \\
&+ \{p_1, p_2, p_3\}^{\mu\nu\rho} D_{310} + \{p_1, g\}^{\mu\nu\rho} D_{311} + \{p_2, g\}^{\mu\nu\rho} D_{312} + \{p_3, g\}^{\mu\nu\rho} D_{313}
\end{aligned}
$$

Then we find,

$$
\begin{aligned}
f_1 &= m_2^2 - m_1^2 - p_1^2 \\
f_2 &= m_3^2 - m_2^2 + p_1^2 - p_5^2 \\
f_3 &= m_4^2 - m_3^2 - p_4^2 + p_5^2 \\
R_{20} &= \frac{1}{2}[f_1 D_0 + C_0(p_5, p_3, m_1, m_3, m_4) - C_0(p_2, p_3, m_2, m_3, m_4)] \\
R_{21} &= \frac{1}{2}[f_2 D_0 + C_0(p_1, p2 + p3, m_1, m_2, m_4) - C_0(p_5, p_3, m_1, m_3, m_4)] \\
R_{21} &= \frac{1}{2}[f_2 D_0 + C_0(p_1, p_2, m_1, m_2, m_3) - C_0(p_1, p_2 + p_3, m_1, m_2, m_4)]
\end{aligned}
$$

$$
\begin{pmatrix} D_{11} \\ D_{12} \\ D_{13} \end{pmatrix} = G_3^{-1} \begin{pmatrix} R_{20} \\ R_{21} \\ R_{22} \end{pmatrix}.
$$

This time the Gram matrix is 3×3,

$$G_3 = \begin{pmatrix} p_1^2 & p_1 \cdot p_2 & p_1 \cdot p_3 \\ p_2 \cdot p_1 & p_2^2 & p_2 \cdot p_3 \cdot \\ p_3 \cdot p_1 & p_3 \cdot p_2 & p_3^2 \end{pmatrix}$$

$$\begin{aligned}
D_{27} &= \frac{1}{(d-3)}[-m_1^2 D_0 - (f_1 D_{11} + f_2 D_{12} + f_3 D_{13} - C_0(p_2, p_3, m_2, m_3, m_4))/2] \\
R_{30} &= \frac{1}{2}[f_1 D_{11} + C_{11}(p_5, p_3, m_1, m_3, m_4) + C_0(p_2, p_3, m_2, m_3, m_4)] - D_{27} \\
R_{33} &= \frac{1}{2}[f_1 D_{12} + C_{11}(p_5, p_3, m_1, m_2, m_4) - C_{11}(p_2, p_3, m_2, m_3, m_4)]] \\
R_{36} &= \frac{1}{2}[f_1 D_{13} + C_{12}(p_5, p_3, m_1, m_3, m_4) - C_{12}(p_2, p_3, m_2, m_3, m_4)] \\
R_{31} &= \frac{1}{2}[f_2 D_{11} + C_{11}(p_1, p_2 + p_3, m_1, m_2, m_4) - C_{11}(p_5, p_3, m_1, m_3, m_4)] \\
R_{34} &= \frac{1}{2}[f_2 D_{12} + C_{12}(p_1, p_2 + p_3, m_1, m_2, m_4) - C_{11}(p_5, p_3, m_1, m_3, m_4)] - D_{27} \\
R_{37} &= \frac{1}{2}[f_2 D_{13} + C_{12}(p_1, p_2 + p_3, m_1, m_2, m_4) - C_{12}(p_5, p_3, m_1, m_3, m_4)] \\
R_{32} &= \frac{1}{2}[f_3 D_{11} + C_{11}(p_1, p_2, m_1, m_2, m_3) - C_{11}(p_1, p_2 + p_3, m_1, m_2, m_4)] \\
R_{35} &= \frac{1}{2}[f_3 D_{12} + C_{12}(p_1, p_2, m_1, m_2, m_3)] - C_{12}(p_1, p_2 + p_3, m_1, m_2, m_4)] \\
R_{38} &= \frac{1}{2}[f_3 D_{13} - C_{12}(p_1, p_2 + p_3, m_1, m_2, m_4)] - D_{27} \\
R_{39} &= -m_1^2 D_0 + C_0(p_2, p_3, m_2, m_3, m_4)
\end{aligned}$$

$$\begin{pmatrix} D_{21} \\ D_{24} \\ D_{25} \end{pmatrix} = G_3^{-1} \begin{pmatrix} R_{30} \\ R_{31} \\ R_{32} \end{pmatrix}.$$

$$\begin{pmatrix} D_{24} \\ D_{22} \\ D_{26} \end{pmatrix} = G_3^{-1} \begin{pmatrix} R_{33} \\ R_{34} \\ R_{35} \end{pmatrix}.$$

$$\begin{pmatrix} D_{25} \\ D_{26} \\ D_{23} \end{pmatrix} = G_3^{-1} \begin{pmatrix} R_{36} \\ R_{37} \\ R_{38} \end{pmatrix}.$$

One point to note is that some of the form factors are overdetermined, in that we find there is more than one possible expression for them in terms of Gram matrix elements and lower rank form factors. This provides a very useful check on the consistency of the calculation, for one must of course get the same answer whichever alternative is used.

$$\begin{aligned}
D_{311} &= \frac{1}{2}m_1^2 D_{11} - \frac{1}{4}[f_1 D_{21} + f_2 D_{24} + f_3 D_{25} + C_0(p_2, p_3, m_2, m_3, m_4)] \\
D_{312} &= \frac{1}{2}m_1^2 D_{12} - \frac{1}{4}[f_1 D_{24} + f_2 D_{22} + f_3 D_{26} - C_{11}(p_2, p_3, m_2, m_3, m_4)] \\
D_{313} &= \frac{1}{2}m_1^2 D_{13} - \frac{1}{4}[f_1 D_{25} + f_2 D_{26} + f_3 D_{23} - C_{12}(p_2, p_3, m_2, m_3, m_4)]
\end{aligned}$$

$$
\begin{aligned}
R_{41} &= \frac{1}{2}[f_1 D_{21} - C_0(p_2,p_3,m_2,m_3,m_4) + C_{21}(p_5,p_3,m_1,m_3,m_4)] - 2D_{311} \\
R_{42} &= \frac{1}{2}[f_2 D_{21} - C_{21}(p_5,p_3,m_1,m_3,m_4) + C_{21}(p_1,p_2+p_3,m_1,m_2,m_4)] \\
R_{43} &= \frac{1}{2}[f_3 D_{21} - C_{21}(p_1,p_2+p_3,m_1,m_2,m_4) + C_{21}(p_1,p_2,m_1,m_2,m_3)] \\
R_{44} &= \frac{1}{2}[f_1 D_{24} + C_{21}(p_5,p_3,m_1,m_3,m_4) + C_{11}(p_2,p_3,m_2,m_3,m_4)] - D_{312} \\
R_{50} &= \frac{1}{2}[f_1 D_{22} - C_{21}(p_2,p_3,m_2,m_3,m_4) + C_{21}(p_5,p_3,m_1,m_3,m_4)] \\
R_{56} &= \frac{1}{2}[f_1 D_{23} - C_{22}(p_2,p_3,m_2,m_3,m_4) + C_{22}(p_5,p_3,m_1,m_3,m_4)] \\
R_{45} &= \frac{1}{2}[f_2 D_{24} - C_{21}(p_5,p_3,m_1,m_3,m_4) + C_{23}(p_1,p_2+p_3,m_1,m_2,m_4)] - D_{311} \\
R_{51} &= \frac{1}{2}[f_2 D_{22} - C_{21}(p_5,p_3,m_1,m_3,m_4) + C_{22}(p_1,p_2+p_3,m_1,m_2,m_4)] - 2D_{312} \\
R_{57} &= \frac{1}{2}[f_2 D_{23} - C_{22}(p_5,p_3,m_1,m_3,m_4) + C_{22}(p_1,p_2+p_3,m_1,m_2,m_4)] \\
R_{46} &= \frac{1}{2}[f_3 D_{24} - C_{23}(p_1,p_2+p_3,m_1,m_2,m_4) + C_{23}(p_1,p_2,m_1,m_2,m_3)] \\
R_{52} &= \frac{1}{2}[f_3 D_{22} - C_{22}(p_1,p_2+p_3,m_1,m_2,m_4) + C_{22}(p_1,p_2,m_1,m_2,m_3)] \\
R_{58} &= \frac{1}{2}[f_3 D_{23} - C_{22}(p_1,p_2+p_3,m_1,m_2,m_4)] - D_{313}
\end{aligned}
$$

$$
\begin{pmatrix} D_{31} \\ D_{34} \\ D_{35} \end{pmatrix} = G_3^{-1} \begin{pmatrix} R_{41} \\ R_{42} \\ R_{43} \end{pmatrix}.
$$

$$\begin{pmatrix} D_{36} \\ D_{32} \\ D_{38} \end{pmatrix} = G_3^{-1} \begin{pmatrix} R_{50} \\ R_{51} \\ R_{52} \end{pmatrix}.$$

$$\begin{pmatrix} D_{37} \\ D_{39} \\ D_{33} \end{pmatrix} = G_3^{-1} \begin{pmatrix} R_{56} \\ R_{57} \\ R_{58} \end{pmatrix}.$$

$$\begin{pmatrix} D_{34} \\ D_{36} \\ D_{310} \end{pmatrix} = G_3^{-1} \begin{pmatrix} R_{44} \\ R_{45} \\ R_{46} \end{pmatrix}.$$

The results so far presented for the form factors were given in the original paper of Passarino and Veltman, and suffice for numerical evaluation of all the necessary form factors. We provide in addition further expressions for some of the form factors, which, as we have explained already, is useful for

the purposes of running self-consistency checks.

$$
\begin{aligned}
Q_1 &= \frac{1}{2}[f_1 D_{25} + C_{23}(p_5, p_3, m_1, m_3, m_4) + C_{12}(p_2, p_3, m_2, m_3, m_4)] - D_{313} \\
Q_2 &= \frac{1}{2}[f_2 D_{25} + C_{23}(p_1, p_2 + p_3, m_1, m_2, m_4) - C_{23}(p_5, p_3, m_1, m_3, m_4)] \\
Q_3 &= \frac{1}{2}[f_3 D_{25} - C_{23}(p_1, p_2 + p_3, m_1, m_2, m_4)] - D_{311} \\
Q_4 &= \frac{1}{2}[f_1 D_{26} + C_{23}(p_5, p_3, m_1, m_3, m_4) - C_{23}(p_2, p_3, m_2, m_3, m_4)] \\
Q_5 &= \frac{1}{2}[f_2 D_{26} + C_{22}(p_1, p_2 + p_3, m_1, m_2, m_4) - C_{23}(p_5, p_3, m_1, m_3, m_4)] - D_{313} \\
Q_6 &= \frac{1}{2}[f_3 D_{26} - C_{22}(p_1, p_2 + p_3, m_1, m_2, m_4)] - D_{312}
\end{aligned}
$$

$$
\begin{pmatrix} D_{35} \\ D_{310} \\ D_{37} \end{pmatrix} = G_3^{-1} \begin{pmatrix} Q_1 \\ Q_2 \\ Q_3 \end{pmatrix}.
$$

$$
\begin{pmatrix} D_{10} \\ D_8 \\ D_9 \end{pmatrix} = G_3^{-1} \begin{pmatrix} Q_4 \\ Q_5 \\ Q_6 \end{pmatrix}.
$$

Bibliography

[1] S. Weinberg, Cambridge, UK: Univ. Pr. (1995) 609 p.

[2] M. E. Peskin and D. V. Schroeder, Reading, USA: Addison-Wesley (1995) 842 p.

[3] G. 't Hooft and M. J. G. Veltman, Nucl. Phys. **B44**, 189 (1972).

[4] Particle Data Group, W. M. Yao *et al.*, J. Phys. **G33**, 1 (2006).

[5] T. Kinoshita, J. Math. Phys. **3**, 650 (1962).

[6] T. D. Lee and M. Nauenberg, Phys. Rev. **133**, B1549 (1964).

[7] F. Maltoni and T. Stelzer, JHEP **02**, 027 (2003), hep-ph/0208156.

[8] F. A. Berends, R. Kleiss, P. De Causmaecker, R. Gastmans, and T. T. Wu, Phys. Lett. **B103**, 124 (1981).

[9] P. De Causmaecker, R. Gastmans, W. Troost, and T. T. Wu, Nucl. Phys. **B206**, 53 (1982).

[10] R. Kleiss and W. J. Stirling, Nucl. Phys. **B262**, 235 (1985).

[11] J. F. Gunion and Z. Kunszt, Phys. Lett. **B161**, 333 (1985).

[12] Z. Xu, D.-H. Zhang, and L. Chang, Nucl. Phys. **B291**, 392 (1987).

[13] M. L. Mangano and S. J. Parke, Phys. Rept. **200**, 301 (1991), hep-th/0509223.

[14] R. Kleiss and W. J. Stirling, Phys. Lett. **B179**, 159 (1986).

[15] L. J. Dixon, (1996), hep-ph/9601359.

[16] E. Witten, Commun. Math. Phys. **252**, 189 (2004), hep-th/0312171.

[17] M.-x. Luo and C.-k. Wen, JHEP **03**, 004 (2005), hep-th/0501121.

[18] G. Georgiou, E. W. N. Glover, and V. V. Khoze, JHEP **07**, 048 (2004), hep-th/0407027.

[19] G. Georgiou and V. V. Khoze, JHEP **05**, 070 (2004), hep-th/0404072.

[20] S. J. Parke and T. R. Taylor, Phys. Rev. Lett. **56**, 2459 (1986).

[21] F. A. Berends and W. T. Giele, Nucl. Phys. **B306**, 759 (1988).

[22] F. Cachazo, P. Svrcek, and E. Witten, JHEP **09**, 006 (2004), hep-th/0403047.

[23] L. J. Dixon, E. W. N. Glover, and V. V. Khoze, JHEP **12**, 015 (2004), hep-th/0411092.

[24] S. D. Badger, E. W. N. Glover, and V. V. Khoze, JHEP **03**, 023 (2005), hep-th/0412275.

[25] Z. Bern, D. Forde, D. A. Kosower, and P. Mastrolia, Phys. Rev. **D72**, 025006 (2005), hep-ph/0412167.

[26] T. G. Birthwright, E. W. N. Glover, V. V. Khoze, and P. Marquard, JHEP **05**, 013 (2005), hep-ph/0503063.

[27] T. G. Birthwright, E. W. N. Glover, V. V. Khoze, and P. Marquard, JHEP **07**, 068 (2005), hep-ph/0505219.

[28] R. Britto, F. Cachazo, and B. Feng, Nucl. Phys. **B715**, 499 (2005), hep-th/0412308.

[29] M.-x. Luo and C.-k. Wen, Phys. Rev. **D71**, 091501 (2005), hep-th/0502009.

[30] R. Britto, F. Cachazo, B. Feng, and E. Witten, Phys. Rev. Lett. **94**, 181602 (2005), hep-th/0501052.

[31] S. D. Badger, E. W. N. Glover, V. V. Khoze, and P. Svrcek, JHEP **07**, 025 (2005), hep-th/0504159.

[32] S. D. Badger, E. W. N. Glover, and V. V. Khoze, JHEP **01**, 066 (2006), hep-th/0507161.

[33] D. Forde and D. A. Kosower, Phys. Rev. **D73**, 065007 (2006), hep-th/0507292.

[34] C. Schwinn and S. Weinzierl, JHEP **03**, 030 (2006), hep-th/0602012.

[35] M. T. Grisaru, H. N. Pendleton, and P. van Nieuwenhuizen, Phys. Rev. **D15**, 996 (1977).

[36] M. T. Grisaru and H. N. Pendleton, Nucl. Phys. **B124**, 81 (1977).

[37] P. Ferrario, G. Rodrigo, and P. Talavera, Phys. Rev. Lett. **96**, 182001 (2006), hep-th/0602043.

[38] G. Rodrigo, JHEP **09**, 079 (2005), hep-ph/0508138.

[39] Z. Bern, L. J. Dixon, D. C. Dunbar, and D. A. Kosower, Nucl. Phys. **B435**, 59 (1995), hep-ph/9409265.

[40] Z. Bern, L. J. Dixon, D. C. Dunbar, and D. A. Kosower, Nucl. Phys. **B425**, 217 (1994), hep-ph/9403226.

[41] C. Quigley and M. Rozali, JHEP **03**, 004 (2006), hep-ph/0510148.

[42] R. K. Ellis, W. J. Stirling, and B. R. Webber, Camb. Monogr. Part. Phys. Nucl. Phys. Cosmol. **8**, 1 (1996).

[43] W. Beenakker, H. Kuijf, W. L. van Neerven, and J. Smith, Phys. Rev. **D40**, 54 (1989).

[44] G. Passarino and M. J. G. Veltman, Nucl. Phys. **B160**, 151 (1979).

[45] J. A. M. Vermaseren, (2000), math-ph/0010025.

[46] S. Catani, S. Dittmaier, and Z. Trocsanyi, Phys. Lett. **B500**, 149 (2001), hep-ph/0011222.

[47] J. G. Korner and Z. Merebashvili, Phys. Rev. **D66**, 054023 (2002), hep-ph/0207054.

[48] LEP Working Group for Higgs boson searches, R. Barate *et al.*, Phys. Lett. **B565**, 61 (2003), hep-ex/0306033.

[49] ALEPH, J. Alcaraz *et al.*, (2006), hep-ex/0612034.

[50] V. A. Khoze, A. D. Martin, and M. G. Ryskin, Eur. Phys. J. **C14**, 525 (2000), hep-ph/0002072.

[51] V. A. Khoze, A. D. Martin, and M. G. Ryskin, Eur. Phys. J. **C23**, 311 (2002), hep-ph/0111078.

[52] A. De Roeck, V. A. Khoze, A. D. Martin, R. Orava, and M. G. Ryskin, Eur. Phys. J. **C25**, 391 (2002), hep-ph/0207042.

[53] J. R. Cudell, A. Dechambre, O. F. Hernandez, and I. P. Ivanov, (2008), 0807.0600.

[54] FP420 R&D, M. G. Albrow *et al.*, (2008), 0806.0302.

[55] B. E. Cox, (2006), hep-ph/0609209.

[56] V. A. Khoze, A. D. Martin, and M. G. Ryskin, Phys. Lett. **B650**, 41 (2007), hep-ph/0702213.

[57] S. Heinemeyer *et al.*, Eur. Phys. J. **C53**, 231 (2008), 0708.3052.

[58] V. A. Khoze, M. G. Ryskin, and W. J. Stirling, Eur. Phys. J. **C48**, 477 (2006), hep-ph/0607134.

[59] S. Weinzierl, (2006), hep-ph/0604068.